Variability of ~~wind~~ surface gravity wave field ~~by~~ over a realistic ~~mesoscale and submesoscale~~ cyclonic eddy~~field~~

Gwendal Marechal[1,*] and Charly de Marez[1,*]

[1]Univ. Brest, CNRS, Ifremer, IRD, Laboratoire d'Océanographie Physique et Spatiale, Brest, France
[*]These authors contributed equally to this work.

Correspondence: gwendal.marechal@ifremer.fr

Abstract. Recent altimeters and numerical studies have shown that ~~wind~~ surface gravity waves interact strongly with ~~small scale~~ small-scale open ocean currents, and subsequently modify ~~their amplitude,~~ the significant wave height, wave frequency, and wave direction. In the present paper we investigate the interactions of ~~wind~~ surface gravity waves with a large and isolated realistic cyclonic eddy. This eddy is subject to instabilities leading to the generation of specific features both at mesoscale and submesoscale. We use the WAVEWATCH III framework to force ~~wind~~ surface gravity waves in the eddy before and after instabilities ~~occurred~~appeared. Our findings show that the spatial variability of wave direction~~frequency and amplitude~~, wave mean period and significant wave height is very sensitive to the presence of ~~underlying~~ submesoscale structures resulting from the eddy destabilisation. As ~~the surface current vorticity~~well as small-scale current structures, the intrinsic frequency of incident waves is key in the wave response of the current modulation, especially for wave direction. Our findings also suggest that surface current gradients ~~can be retrieved thanks to~~ could be approached thanks to significant wave height gradients ~~at scale where traditional altimeter measurements fail~~measurements until very small spatial resolution. However it is difficult to have information on the phase of those current gradients due to the non-local effects of currents on waves.

1 Introduction

The ubiquity of mesoscale (10-100 km) and submesoscale (1-10 km) eddies, fronts, and filaments at the superficial layer of the ocean induces a strong variability in the wave field generated by wind (waves): waves-current interactions result in a change of ~~wave height~~significant wave height (H_s), frequency, and direction ~~(Phillips, 1977; Mei, 1989)~~(Phillips (1977) and Mei (1989)). From these modulations, it has been proved recently, thanks to both ~~numerical simulations and field measurements~~ field measurements and numerical simulations, that the ~~effect~~ effects of currents on waves ~~induces a strong regional inhomogeneity~~ induce strong regional inhomogeneities of the wave field (Romero et al., 2017, 2020). In particular, Ardhuin et al. (2017) showed thanks to realistic numerical simulations that the ~~wave height~~ H_s variability is closely linked to surface Kinetic Energy (KE) at mesoscale. Quilfen et al. (2018); Quilfen and Chapron (2019) used high resolution ~~wave height~~ H_s measurements from altimetry to highlight the close link between current ~~gradient and wave height gradient~~gradients (∇ U) and significant wave height gradients (∇H_s). Villas Bôas and Young (2020) proved, in the absence of wave dissipation and wind momentum input~~that the gradient~~, that the gradients of the wave direction induced by current is necessarily induced by the solenoidal component of the surface ~~current~~ currents (vorticity). Finally, Villas Bôas et al. (2020), under the same assumptions, ~~emphasised~~ emphasized the narrow link between ~~surface vorticity and the wave height gradient. Besides, surface~~ the surface vorticity of the flow and the ∇H_s. Surface currents seem to increase the deep-water breaking wave probability (Romero et al., 2017, 2020). ~~The wave~~ Wave breaking at the air-sea interface is the major source of momentum and heat exchange between ~~wave~~ waves and currents (Cavaleri et al., 2012) or ~~gaz~~ gas and sea spray production ~~(Monahan et al., 1986). Surface~~ (Monahan et al., 1986; Bruch et al., 2021). That is why surface mesoscale and submesoscale currents, through their ~~interaction with the wind~~ interactions with the wave field, ~~thus~~ have a significant impact on ~~gas and heattransfers between the ocean and the atmosphere.~~

~~In mesoscale surface current field as *e.g.* at boundary currents (Gulf Stream, Agulhas current, Drake passage~~air-sea fluxes (momentum, gas, heat, sea-spray, ...)~~the wave height gradients are mostly due to refraction (change of wave direction, see Irvine and Tilley (1988); Ardhuin et al. (2017); Marechal and Ardhuin (2021)). Indeed mesoscale and submesoscale eddies redistribute spatially the wave action and subsequently generate wave energy convergence and divergence. This explains the strong wave height gradients measured in those current regimes. The same result has also been highlighted for waves propagating in a synthetic current, fully or partially solenoidal, and very turbulent, at scales between 15 and 200 (White and Fornberg, 1998; Villas Bôas et a~~

.

In the ocean ~~, the ubiquity of eddies is no longer to be proven~~ and particularly in western boundary currents, eddies are ubiquitous from mesoscale to submesoscale (Chelton et al., 2007, 2011; Gula et al., 2015b; McWilliams, 2016; Rocha et al., 2016). The interaction between ~~such coherent structures~~ eddy field and waves is thus of primary importance for the global distribution of wave properties. In the present study, we analyse numerically the effect of ~~a~~ an isolated realistic eddy on the wave properties (~~amplitude, frequency~~H_s, mean period, and direction). Former similar works ~~already performed such analysis~~have been already performed, but only ~~in~~ for idealized eddy cases (Gaussian profiles, see Gallet and Young (2014); Mapp et al. (1985); Mathiesen (1987); White and Fornberg (1998); Holthuijsen and Tolman (1991)). However, the structure of eddies in the ocean can strongly differ from textbook analytical idealized profiles (Le Vu et al., 2018; de Marez et al., 2019), ~~such as Gaussian ones,~~ making the study of waves-Gaussian eddy an unrealistic framework. ~~Furthermore,~~ Indeed, the instabilities occurring in a large and isolated eddy result in the strong production of energy in the oceanic submesoscales range (Hua et al., 2013; de Marez et al., 2020b) which would interact strongly with waves. Furthermore, most of the previous studies solely focused on the refraction induced by ~~eddies without discussing the wave height gradients resulting from the interaction~~ (**?**)0pt~~GalletYoung2014~~an eddy without discussing on the modulation of wave parameters (H_s or mean wave period, Gallet and Young (2014); Mapp et al. (1985); White and Fornberg (1998)). Here, our goal is to investigate the long-term mean effects of an isolated cyclonic eddy with a realistic shape (highly dynamic at meso- and submesoscale) on the wave properties. We demonstrate that wave field characteristics are strongly modified by the presence of the eddy and that the variabilities are more important as the eddy field is multi-scale dynamic. In a real ocean, the resulting deviation of the waves from the great circle path due to eddy-induced refraction are thus certainly underestimated when eddies are considered as gaussian (Gallet and Young, 2014; Smit and Janssen, 2019) as well as extreme wave height waves in eddy that can be found in the vicinity of main branches of western boundary currents, ~~Mathiesen1987, WhiteFornberg1998). The~~

~~investigation of wave height variability induced by surface currents is crucial for the anticipation of extreme waves in mesoscale currents(Lavrenov, 1998; Hasselmann et al., 2012), and for remote sensing application where wave height gradients induce a sea states bias (Fu and Glazman, 1991). ?Villas Bôas et al. (2020)~~ e.g in the Gulf-Stream (Holthuijsen and Tolman, 1991). Also, the estimated ocean circulation from altimeters measurements are affected by noise correlated to the H_s. Some proposed methods to remove the contribution of waves in altimeters measurements assume that the wave field is sufficiently smooth under 200 km (Sandwell and Smith, 2005). Focus on H_s variability over a realistic eddy field pattern (more realistic than a gaussian eddy) will reveal very sharp wave parameter gradients thus making the assumption that wave field homogeneous at the scale of hundred kilometers not acceptable. Finally, previous works showed that wave ~~height gradients and surface current gradients are closely linked, the investigation of how wave height follows the underlying current signal seems to be promising to allow the surface current retrieval without any direct measurements~~characteristic can be inverted to infer surface currents intensity (Huang et al., 1972; Sheres et al., 1985) or more recently Villas Bôas et al. (2020). The last study showed that sharp emerging $\nabla \mathrm{H}_s$ can be inverted to infer the $\nabla \mathrm{U}$ that have generated them. In the same framework of Villas Bôas et al. (2020) we will show that the amplitude of $\nabla \mathrm{U}$ can be approached by inverting the variabilities of the wave field induced by the eddy field. Reconstruct the ∇U field would be fruitful for a wide range of applications (search and rescue, plastic debris monitoring, biological activities or short-term wave forecast).

The manuscript is organised as follows. In section 2, we introduced the eddy structure used in the study, based on the work of de Marez et al. (2020b), and the numerical ~~model built from Ardhuin et al. (2017)~~ framework WAVEWATCH III (The WAVEWATCH III® Development Group, 2016) without source terms. In section 3, we present the results of the numerical experiments. ~~Finally, in~~ In section 4, we discuss on how significant wave height and current ~~gradient~~ gradients are coupled. ~~Potential~~ In section 5 we investigate quickly the effects of nonlinear wave-wave interactions on the intensity of the wave parameter gradients. Limits and perspectives of this present work close ~~this~~ the manuscript.

2 Method

2.1 ~~The realistic~~ A cyclonic eddy from in-situ measurements

To study the wave propagation through ~~a realistic eddy , we use~~ an eddy field, we used the outputs of the simulation performed by de Marez et al. (2020b). In this study, authors performed ~~spindown~~ idealized simulations, using the Coastal and Regional Ocean COmmunity model, CROCO (Shchepetkin and McWilliams, 2005), that solves the hydrostatic primitive equations (PE) for the velocity $\mathbf{u} = (u, v, w)$, temperature T, and salinity S, using a full equation of state for seawater (Shchepetkin and McWilliams, 2011). ~~Details of the parameterization are fully described in de Marez et al. (2020b).~~

The spatial resolutions are chosen to accurately resolve both the frontal dynamics and the forward energy cascade at the surface. The simulation is initialised with a composite cyclonic eddy as revealed by Argo floats in the northern Arabian Sea (details of the composite extraction are fully described in de Marez et al. (2019)). The eddy is intensified at the surface, but has a deep-reaching influence down to about 1000 m depth. Its initial horizontal shape corresponds to a shielded vorticity monopole: a positive core of vorticity and a shield of negative vorticity (Fig. 1(a)). Its radius, $R = 100$ km, is large compared to the mean regional Rossby radius R_D (47 km, see Chelton et al. (1998)). It is a mesoscale eddy. In the following, mentions to "submesoscale" ~~refer~~ refers to features and processes occurring at scales that are small compared to ~~R_D~~ Rossby deformation radius (*i.e.* $Bu > 1$ ~~).~~

~~During the simulation,~~ with $Bu = \frac{R_D^2}{L^2}$). de Marez et al. (2020b) observed that the eddy is unstable with respect to a mixed barotropic/baroclinic instability. The latter deforms the eddy, which eventually evolves into a tripole after about 4 months of simulation. Sharp fronts are subsequently generated in the surface mixed layer at the edge of the tripole. These fronts then become unstable, and this generates submesoscale cyclones and filaments. Near these fronts, diapycnal mixing occurs, causing the potential vorticity to change sign locally, and symmetric instability to develop in the core of the cyclonic eddy. Despite the instabilities, the eddy is not destroyed and remains a large-scale coherent structure for one year of simulation. A full description of instability processes can be found in de Marez et al. (2020b). ~~Thus, the final state of the simulation (*i.e.* after about half a year of simulation , see~~ Snapshots of the current velocity and vorticity of the fully developed eddy field after 210 days of simulation are represented in Fig. 1b ~~) represents well a realistic turbulent vorticity field surrounding an eddy in the ocean: the~~ and d respectively. The main core of the cyclone is surrounded by filaments, submesoscale eddies and fronts, that lead to sharp vorticity gradients. This vorticity field is far from the usual idealised representation of eddies often considered in the literature, and is closer to reality (see *e.g.* Fig. 1 in Lévy et al. (2018) for an example of a realistic turbulent field above mesoscale eddies).

For the purpose of the present study, we consider the surface velocity fields (the simulated level closest to the ocean surface) from the simulation outputs described above. We use the initial state that represents the eddy before instabilities occur (Fig. 1(a)), and the state after 210 days of simulation, in which submesoscale features have been generated by the spontaneous instability of the eddy (Fig. 1(b)). At 210 days all instabilities have occurred (mixed barotropic/baroclinic instabilities). After 210 days the eddy field starts to dissipate making some small-scales features disappear (de Marez et al., 2020b). Please notice that the use of strictly 2D surface current is an approximation of what happen in the nature. In reality, waves feel the effects of an "average current" integrated over a certain depth along the first meters of the water column. This depth depends on the wavelength of the waves (Kirby and Chen, 1989).

2.2 The wave model

To describe the ~~dynamics of waves passing through~~ dynamic of waves over the eddy described above, we use the WAVEWATCH III framework (The WAVEWATCH III® Development Group, 2016) ~~. This~~ forced both by the initial state of the eddy (gaussian shape, Fig.1a,c) and the fully developed eddy (Fig.1b,d). The model integrates wave action equation

$$\partial_t N(\sigma,\theta) + \nabla.(\dot{x}N(\sigma,\theta)) + \partial_k(\dot{k}N(\sigma,\theta)) + \partial_\theta(\dot{\theta}N(\sigma,\theta)) = S, \tag{1}$$

where $N(\sigma,\theta)$ is the wave action ($N(\sigma,\theta) = \frac{E(\sigma,\theta)}{\sigma}$, with $E(\sigma,\theta)$ the two dimensional wave energy spectrum), θ is the wave direction of propagation, $\dot{x}$ is the wave action advection velocity (equal to the sum of the wave group and the surface current ~~vectors), and~~ velocity), $\dot{k}$ and $\dot{\theta}$ are the wave advection ~~velocity~~ velocities in the spectral space ~~, their expressions~~ The expressions of $\dot{k}$ and $\dot{\theta}$ are developed from wave ray equations ~~which describe the wave kinematic~~ (Eq.3) and are fully given in (Phillips, 1977; Benetazzo et al., 2013; Ardhuin et al., 2017). The right hand side of Eq. (1) is the sum of the source terms

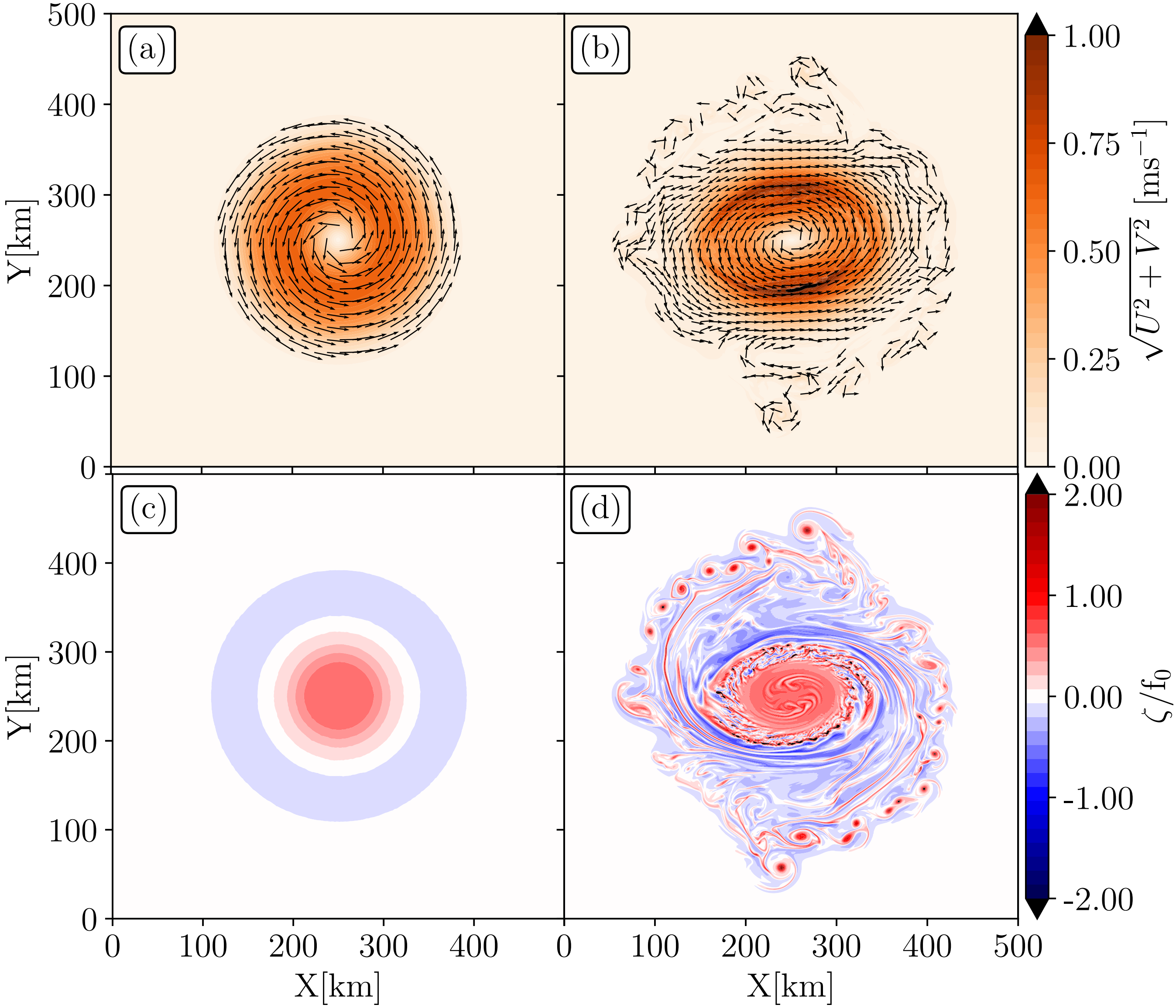

Figure 1. ~~Normalized relative vorticity from de Marez et al. (2020b)'s simulation outputs~~ Surface currents intensity and direction for the initial/gaussian eddy (~~$f_0 = 5.2\,10^{-5}\,\mathrm{s}^{-1}$ at 23°N)~~ panel (a)~~at initialisation and (b~~) and after ~~destabilisation (~~210 days of ~~simulation~~destabilization (panel (b)~~, as used~~). Their associated normalized relative vorticity ($\zeta = \partial_x V - \partial_y U$) are given in panel (c) and (d). The Coriolis parameter is kept constant in the ~~wave model integration~~simulations: $f_0 = 5.2\,10^{-5}\,\mathrm{s}^{-1}$. The original zonal and meridional velocities (de Marez et al., 2020b) have been here multiplied by two.

describing the wind energy input, the dissipation due to wave breaking and bottom friction, and the ~~non-linear~~ nonlinear energy exchange between waves. ~~For this study we consider already well developed waves, propagating in the current field without any source term (no dissipation, no non-linear exchange, and no wind input, *i.e.* $S = 0$).~~

In a current field, it is necessary to consider a non-Galilean frame of coordinate (moving frame of reference). The ~~wind~~ waves dispersion relationship is thus impacted because the current induces a Doppler shift ~~of~~ on the wave frequency (Eq.(2)),

$$\omega = \sigma + \mathbf{k}.\mathbf{u}. \tag{2}$$

~~where~~ The wave ray equation is also modified,

$$\partial_t \mathbf{k} = \partial_{\mathbf{x}} \omega. \tag{3}$$

ω is the absolute frequency, $\mathbf{k}$ the wavenumber vector, $\mathbf{u}$ the surface current vector, σ the intrinsic wave frequency ~~and~~ equal to $\sqrt{gk}$ in deep water (where water depth is largely greater than wave wavelength, here k is a scalar) ~~,~~ and g is the gravity acceleration~~and **u** is the surface current vector~~. Bold characters refer to vector notation all along this manuscript. For this study we consider waves already well developed, far from their generation areas, propagating in the current field without any source term (no dissipation, no nonlinear exchange between waves, and no wind input, i.e. the right hand side of Eq.(1) is equal to 0). The aim of the current study is to investigate, in a very idealized case, how long waves properties can be modified by an eddy field more realistic than an isolated and gaussian eddy. In a more realistic framework, the waves steepness modified by the current or due to non initial waves-waves interactions would trigger local wave breaking as observed in Romero et al. (2017) . Also wind input would generate higher frequency waves which will also interact with the eddy field. In a fully coupled simulation, the currents itself would be modified due to the presence of the waves at the air-sea interface.

Throughout this manuscript we discuss the evolution of the ~~significant wave height (~~H_s ~~)~~ and the mean wave period weighted on the low frequency part of the wave spectrum ($T_{m0,-1}$), known as "bulk" quantities. We called them "bulk" because they are ~~summed~~ integrated over the wave energy spectrum $E(\sigma,\theta)$.

They are defined as

$$H_s = 4\sqrt{\int\limits_{\theta}\int\limits_{\sigma} E(\sigma,\theta)\, d\sigma d\theta}, \tag{4}$$

and

$$T_{m0,-1} = \frac{1}{\int_\theta \int_\sigma E(\sigma,\theta) d\sigma d\theta} \int\limits_{\theta}\int\limits_{\sigma} \sigma^{-1} E(\sigma,\theta) d\sigma d\theta. \tag{5}$$

The evolution of the wave peak direction (θ_p, θ where $E(\sigma,\theta)$ is maximum) ~~is also studiedwhile waves are travelling in the current field. The performances~~ has been also studied. The performance of the wave model used here ~~have~~ has already been discussed in boundary currents systems such as the Gulf Stream, ~~the Agulhas current, or the Drake Passage~~ Drake Passage and Agulhas current, especially concerning the H_s estimation (Marechal and Ardhuin, 2021; Ardhuin et al., 2017). In those previous studies, wind forcing, waves dissipation, and nonlinear wave-wave interactions have been taken into account.

We ~~initialize~~ initialized simulations with waves that are propagating from the ~~west side~~ left boundary of a 500×500 km Cartesian domain, with a resolution of 500 m both in ~~meridional and zonal direction. Spectral model is initalized with a narrow band spectrum of frequency spreading on 0.03 ,~~ horizontal and vertical directions. The right boundary is open. The initialization is done with a narrow-banded wave spectra gaussian in frequency centered at varying peak frequencies, f_p=0.1428 Hz, 0.097 Hz, and 0.0602 Hz. The ~~frequencies are~~ spectral energy spectrum has a frequency spreading of 0.03 Hz around the peak frequency and $H_s = 1$ m. The frequencies have been chosen to correspond to the mean periods used in the work of Villas Bôas et al. (2020) (7 s, 10.3 s, and 16.6 s). ~~At initialization, $H_s = 1$ m~~Waves are generated at the left boundary, from spectra described above, every hour. The initial direction of waves is 270°. The direction convention follow the meteorological convention such that 270° waves are coming from the left and 0° waves are coming from the top of the domain. The wave field reaches a stationary state after 09:15, 08:45, and 07:30 of simulation for initializations of T_p=7s, T_p=10.3 s, and T_p=16.6 s, respectively, we recall that source terms have been removed and the current field assumed stationary. The wave model global time step is 12 s, the spatial advection time step is 4 s, and the spectral time step is 1 s. The model provide outputs every fifteen minutes. Wave spectra are computed at each grid point, discretized into ~~48 directions and~~ 32 frequencies ~~. Indeed, dealing with high directional resolution allows~~ and 48 directions. High directional resolution is required for a better description of wave refraction, especially in strong rotational current (Ardhuin et al., 2017; Marechal and Ardhuin, 2021). ~~As mentioned above, surface currents are added in wave propagation simulations. These surface currents~~ The surface current forcing fields are from de Marez et al. (2020b)'s simulations output. In one case we considered the initial shape of the cyclonic eddy (Fig. 1(a,c)). In the other case, we considered the ~~turbulent~~ fully developed state of the cyclonic eddy (Fig. 1(b,d)). In the following, this cases are called the ~~unperturbed and the perturbed~~ initial and the fully developed cases, respectively. The initial eddy case is similar to the former works performed over analytical eddy (Mathiesen, 1987; Holthuijsen and Tolman, 1991; White and Fornberg, 1998; Gallet and Young, 2014). The variation timescale of the current is much longer ($\mathcal{O}(1)$ week) than the ~~wave one~~ waves (($\mathcal{O}(1)$ minute)~~, thus respecting~~ . So it respects the steady current assumption during one wave train propagation. The eddy described in previous section and in de Marez et al. (2020b) is an averaged composite eddy reconstructed from measurements in the Arabian Sea (de Marez et al., 2019). The method of reconstruction tends to an underestimation of the eddy intensity~~. Hence,~~ , that is why the intensity of the current has been multiplied by ~~five~~ two to increase the potential effects of ~~current~~ currents on wave properties~~, while~~ . The eddy is staying geophysicaly realistic (current velocity remains around ~~2.5~~ 1 m.s^{-1} ~~). This strategy is comparable to the one presented~~ and normalized vorticity lower than 2, Fig.1). Those values are comparable with surface vorticity measured in the first hundred meters of Arabian sea (de Marez et al., 2020a) and in other current regimes as in the western boundary currents (Tedesco et al., 2019; Gula et al., 2015a). Although the eddy field represented in Fig.~~10 of Gallet and Young (2014)~~1 is from an averaged composite eddy (solely estimated using in-situ data), it has been considered, in this study, as realistic because differs from an analytical vortex. Also, it has been compared with altimeter and drifter data in the region where it has been estimated. The cyclonic eddy was coherent with those measurements (see Fig.12, 13, and 14 of de Marez et al. (2019)).

3 Wave field variability in a cyclonic and realistic eddy

The frequency sensibility of the incident waves is studied ~~in both the unperturbed and the perturbed cases.~~ both in the initial and in the fully developed eddy. Waves are dispersive in deep water~~and are propagating in the current~~, their group and their energy propagates at the group velocity (C_g). For T_p=7 s ($T_p= \frac{1}{f_p}$)~~wave packet is propagating slower than~~, T_p=10.3 s ~~which are propagating slower than~~ and T_p=16.6 s~~waves ($C_g \sim$~~, group velocity are 11, 16, and 26 m.s^{-1}~~respectively)~~. To reach X=X$_0$ (a given ~~longitude~~value of horizontal scale) shorter waves take more time than longer waves. ~~The snapshots presented in~~ As waves are generated continuously from the left boundary a stationary state is reached after a sufficiently long simulation time. In Figs. 2, 3, and 4 ~~are thus taken for three different time outputs depending on T_p of the incident waves (t=105 , 90 and 75 respectively)~~fields are taken once the stationary state is reached. Surface currents modulate ~~amplitude, frequency and~~ the wave amplitude, the wave frequency and the waves direction, the variability of those quantities are highlighted through H_s, $T_{m0,-1}$, and θ_p fields. The ~~respond~~ response of other waves ~~parameters for a prescribed~~ variability for this underlying current, as the directional spreading or the mean direction, are not described in this manuscript.

3.1 Modulation of wave parameters

3.1.1 Significant wave height

Surface currents induce a strong regional H_s variability, specially in a highly solenoidal field ~~(Marechal and Ardhuin, 2021). Wave train is propagating from the west boundary with an initial direction of 270° (0° is the geographical North, and the direction convention is where waves are propagating)~~(Ardhuin et al., 2017; Villas Bôas et al., 2020). Outputs of wave simulation performed in the ~~unperturbed and perturbed eddy is~~ initial and in the fully developed eddy are given in Fig. 2. The presence of an underlying vortex induce ~~a strong wave height gradient (~~strong ∇H_s~~)~~, inside and outside the eddy. ~~Model~~ Simulations forced with the ~~unperturbed~~ initial eddy (2a,b,c) ~~shows~~ show coherent alternate sign H_s structures along meridians (fixed X−axis). An important lens shape dipole of H_s ~~enhancement~~ increase and decrease is noticeable in the field. H_s reaches a maximum of ~~1.6 , 1.4 , 1.2~~ 1.62 m ~~(60, 40, 20 % enhancement with respect to the initial H_s) at X=250~~ at X=333 km ~~, Y= 300~~ and Y=311 km for ~~simulations initialized with~~ simulation initialized at T_p=7 ~~,~~sec, 1.62 m at X=349 km and Y=310 km for simulation initialized at T_p=10.3 ~~and~~ sec, and 1.57 m X=365 km and Y=310 km for simulation initialized at T_p=16.6 ~~respectively (~~sec. A transect at X=300 km is given for each initialization in Fig. 2g~~). A secondary~~. Two maximums are noticeable, the main one at Y=310 km and a secondary at Y=125 km. Two minimum are noticeable, one at Y=200 km (H_s~~maximum is apparent at the southernmost part of the domain (enhancement of ∼ 20%)at X =300 , Y= 75~~ = 0.8 m) and a secondary one within Y=380 km (H_s=0.85 m). One can see that more incident waves are short more are the extremes values measured at constant X. Globally, H_s follows the current vorticity signal (Fig.1c). The enhanced H_s areas are associated to the boundary of the inner eddy core ($\zeta > 0$) and the vorticity ring ($\zeta < 0$) that surround the ~~principal structure. Decrease of H_s is also apparent in the field, specially in the core of the eddy (∼ -40% decrease with respect to the initial H_s) with a scattering of the signal easterly of X=300 within Y=150,300in two large tongues. The decrease of H_s at X=250 are identical for simulations forced with the unperturbed eddy (Fig. 2g) for each wave model's initialization. Globally where~~ eddy core. Where waves are

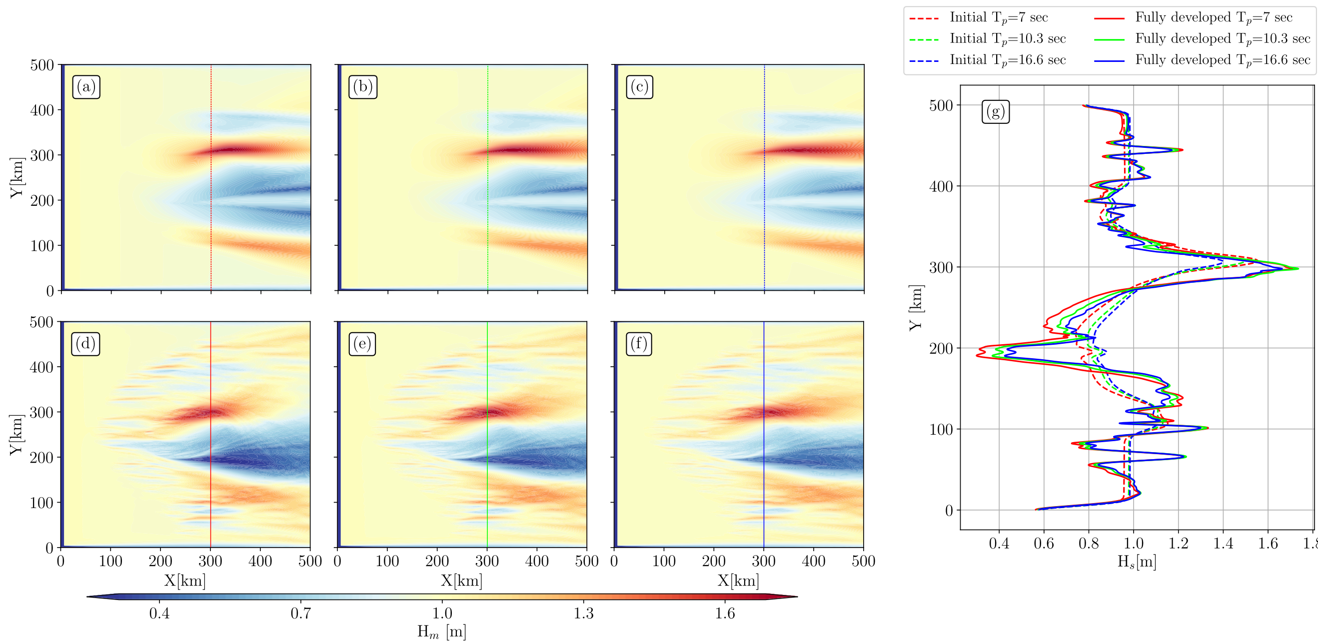

Figure 2. ~~Instantaneous significant~~ Significant wave height ~~field~~ (H$_s$) fields for (a,d) T$_p$=7 s, (b,e) 10.3 s, and (c,f) 16.6 s incident waves. ~~The initial wave field~~ Without current forcing the entire domain is ~~initialized at~~ equal to the initial H$_s$ ~~=1 m~~(1m). The first ~~line~~ row (a,b,c) shows ~~instantaneous field~~ fields for simulations forced with the ~~unperturbed~~ initial eddy (Fig. 1(a,c)); the second ~~line~~ row (d,e,f) shows the same ~~instantaneous field~~ fields but for simulations forced with the ~~perturbed~~ fully developed eddy (Fig1(b,d)). Panel (g) shows ~~significant wave height~~ H$_s$ along X = ~~250~~ 300 km (colored dashed~~line~~/solid lines in ~~panel (a)~~left panels) for all simulations.

propagating against the current, H$_s$ is enhanced which agree with waves-eddies interactions simulated in realistic fields ; (see Fig. 6 of Romero et al. (2020) and Fig.1 of Ardhuin et al. (2017)).

~~Model forced with perturbed eddy shows stronger spatial inhomogeneity~~ Simulations forced with fully developed eddy show stronger spatial inhomogeneities in the wave field (Fig. 2d,e,f). As noticed for simulations forced with the ~~unperturbed~~ initial eddy (2a,b,c), the H$_s$ field is matching pretty well with the ~~current forcing used~~ cuusedrrent forcing (Fig. 1b), in other word where surface current gradients are important, strong ∇H_s are noticed. H$_s$ is mostly modulated by the ~~center structure of the perturbed eddy. Nevertheless, significant ∇H_s are occurring~~ fully developed eddy core. The modulation of H$_s$ by the eddy core occurs $\sim$ 50 km more upstream (smaller X value) than for simulations forced with initial eddy. Let us notice that ∇ H$_s$ are apparent in the submesoscale eddies that have been emerged spontaneously all around the ~~center structure~~ eddy core. In the submesoscale eddy field, wave field show alternate sign of H$_s$ variabilities, with globally the same intensity whatever the incidence frequency. It is explicitly shown in Fig. 2g at Y<180 km and Y> 350 km ~~. Wave actions in the perturbed eddy is~~ for each initialization. In the same transect, at Y=200 km, we can do the same remark as previously, more incident waves are short more ∇H_s are sharp. However at X=300 km and at Y corresponding to submesoscale eddies, the ∇ H$_s$ are identical whatever the initialization of waves. The H$_s$ in the fully developed eddy are more scattered (mostly zonally due to the initial direction of the incident wave packet) than in the ~~unperturbed eddy. Wave height is also larger at X=250 , Y=300 and smaller at X=300 , Y=200 than in perturbed eddysimulations~~initial eddy. ∇H_s ~~is globally the strongest for simulations initialized with T$_p$=7 wave packet~~ are sharper for simulations forced with the fully developed eddy and higher extreme values are reached. One can see that ∇H_s are important dowstream the eddy field. The horizontal size of H$_s$ patches (intensified or decrease H$_s$ structures) are comparable to the width of the eddy (Fig.~~2a,d,g)than in simulations with T$_p$=10.3 and T$_p$=16.6~~ 4a-f). Finally one can see that for all simulation the signature of the eddy in the H$_s$ field is not totally symmetric whereas the two forcing current field seemed to be so.

3.1.2 Peak direction

The ~~refraction induced by the surface currents~~ effect of currents on wave directions can be captured ~~at~~ to the first order by the θ_p field. Waves are turning in the current field due to refraction, globally toward the South (θ_p ~~decreases~~increase) in the bottom part of the domain and toward the North (θ_p ~~increases~~decreases) in the upper part.

When waves pass through the eddy, θ_p changes due to the vorticity field, at X~~= 125~~ =125 km for the ~~unperturbed~~ initial eddy (Fig.3a,b,c), ~~slightly upwind for the perturbed eddy; at X= 90~~ and slightly upwind, at X=79 km, for the fully developed eddy (Fig.3d,e,f). Patterns showed in Fig. 3 are similar to the H$_s$ gradient patterns showed in Fig. 2 with a ~~large scale dipole for simulation forced with unperturbed~~ large-scale dipole for simulations forced with initial eddy and both ~~a large scale and small scale signal gradient~~ large-scales and small-scales signal gradients for simulations forced with the ~~perturbed eddy. The large~~ fully developed eddy. Narrow yellow bands in the left part of each panels are spurious~~.~~

, they marked the boundary where waves are generated at the left boundary. The peak direction gradient ($\nabla\theta_p$) intensity ~~is function of both~~ depends both on the incident wave frequency and the underlying vorticity field (Dysthe, 2001; Kenyon, 1971). $\nabla\theta_p$ is stronger for simulations initialized with T$_p$=7 s (Fig. 3a,d) than for simulations initialized with T$_p$=10.3 s and 16.6 s. In the same way, $\nabla\theta_p$ is enhanced for simulations forced with ~~perturbed~~ the fully developed eddy (Fig. 3d,e,f)) where current field ~~is more turbulent. This~~ shows more smaller current features. The result corroborates Villas Bôas et al. (2020)'s findings where authors forced wave model with synthetic surface ~~current inverted from KE~~ currents inverted from Kinetic Energy spectrum (with a random phase). The more turbulent the current was~~turbulent~~, the more waves ~~scattered with convergence and divergence areas of wave trajectories, like a random walk. These areas of convergence and divergence of waves trajectory are discussed later in this manuscript. In the presence of current, waves follow the Fermat principle, in the geometric optic framework waves take the shortest path to join two distant areas.For linear waves in deep water the curvature of wave ray is proportional to $\frac{\zeta}{C_g}$, with ζ the current vorticity and C_g the wave group velocity.~~

~~Villas Bôas and Young (2020) demonstrated that in the absence of forcing and dissipation, waves are scattered by the rotationnal components of the current. The current field used as model forcing is highly rotational (de Marez et al., 2020b).~~ were refracted. Refraction can induce a change of θ_p that can reach $\pm$ 30° for simulation initialized by T$_p$=7 sec and forced with the fully developed eddy (Fig.3d). Very long waves trains (T$_p$=16.6 sec) hardly reach a deviation of wave direction higher than 10°, both

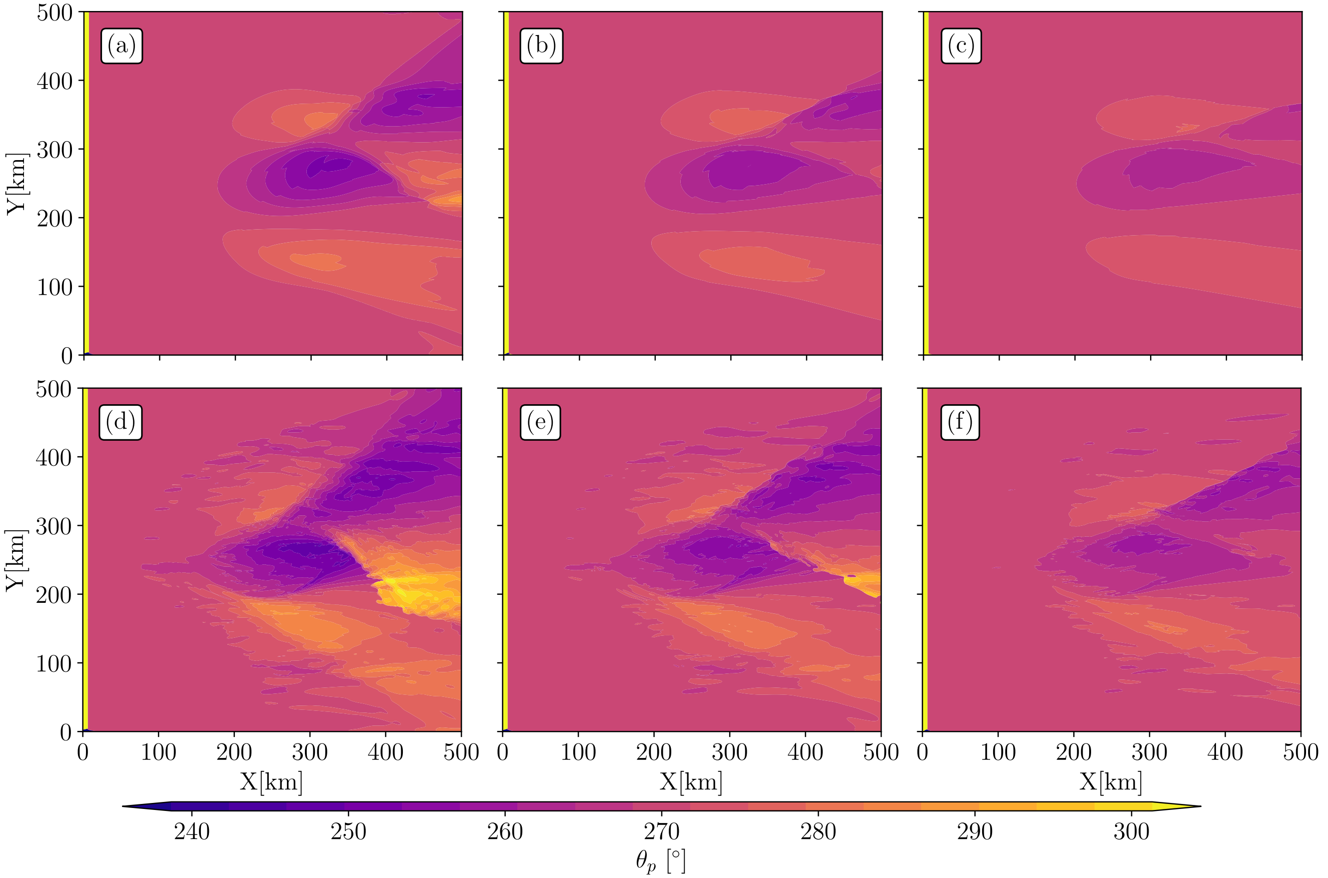

Figure 3. ~~Instantaneous peak~~ Peak direction (θ_p) field for (a,d) T_p=7 s, (b,e) 10.3 s, and (c,f) 16.6 s incident waves. ~~The initial wave direction, at X=0~~ Without current forcing the entire domain is equal to the initial θ_p ~~=~~(270°). The first ~~line~~ row (a,b,c) shows ~~instantaneous field~~ fields for simulations forced with the ~~unperturbed~~ initial eddy (Fig. 1(a,c)); the second ~~line~~ row (d,e,f) shows the same ~~instantaneous field~~ fields but for simulations forced with the ~~perturbed~~ fully developed eddy (Fig. 1(b,d)).)

in fully developed and initial eddy. Finally one can see that θ_p differs downstream the eddy with respect to the initial direction (270°), waves keep in memory the effects of surface currents

3.1.3 Mean wave period

As surface currents have an effect on the wave frequency (Phillips, 1977) due to the conservation of the absolute frequency, Eq.(2), surface currents modified $T_{m0,-1}$. Wave simulations are initialized with different wave ~~train~~ peak frequencies, ~~thus impacting~~ so directly impacting the values of $T_{m0,-1}$.

The different initializations of the wave field justify the representation of the relative difference of $T_{m0,-1}$ (Δ $T_{m0,-1}$) rather than raw outputs. This Δ $T_{m0,-1}$ is the difference between outputs of simulations performed with and without surface current forcing (Fig.4). At first glance, the spatial ~~inhomogeneity is~~ inhomogeneities are more striking for ~~simulation~~ simulations forced with the ~~perturbed eddy, similarly as for~~ fully developed eddy, similar to the H_s ~~instantaneous~~ and θ_p fields (Fig. 2~~).~~

~~As waves are dispersive, longer waves are faster than short ones resulting in a large scale zonal gradient of~~ , 3). For a fully developed eddy, Δ $T_{m0,-1}$ ~~. Qualitatively, waves are globally shorter (smaller~~ exceeds 3 sec in the eddy core for X between 200 km and 400 km. For initial eddy forcing Δ $T_{m0,-1}$ ~~) where~~ does not goes above 2 sec at the same location (Fig 4g). As for H_s ~~is enhanced (Fig. 2)~~field, the Δ $T_{m0,-1}$ does not much depend on the frequency of the incident waves, or at least, not as much as $_{t}heta_{p}$ field studied above. Slight differences are however noticeable for simulations forced with fully developed eddy. This is ~~mostly the case where current is in the opposite direction than the wave propagation direction . Indeed, as currents~~ not clear if there is a link between the incident wave frequency and the slight differences in Δ $T_{m0,-1}$ signal especially in the submesoscale eddies where Δ $T_{m0,-1}$ are stronger for long incident waves whereas we see the opposite in the core of the fully developed eddy. Δ $T_{m0,-1}$ are positive where waves and current are propagating in the same direction and vice versa. This change of Δ $T_{m0,-1}$ is because current induce a Doppler shift on the wave frequency (Eq.(2)~~, where~~) and that the absolute frequency is conserved. Where waves and current are opposite ~~, waves are shortened~~ we see that H_s are enhanced (Fig.2) and waves wavelength are shortened. It is due to the conservation of wave action ($D_t N = 0$, Eq. (1)) ~~. Waves and currents also exchange their energy by conservation of absolute frequency~~If we focus on the maximum of Δ $T_{m0,-1}$ at Y=200 km, waves are extended of about 153 m and H_s decreased of about 0.65 cm. One can see that waves stripes induced by refraction (Fig. 3) are also captured in the mean wave period signal and that waves are shorter (smaller $T_{m0,-1}$) where H_s were enhanced (Fig. 2). We precise that the change of H_s induced by current is due to a superposition of processes~~as explicitly described in Ardhuin et al. (2017); Quilfen et al. (2018); Kudryavtsev et al. (2017b) and all along this manuscript.~~

~~Finally we guess that in a fully diverging current , $T_{m0,-1}$ fieldwould be more impacted, as described in Villas Bôas et al. (2020) . The waves stripes induced by refraction (Fig. 3)is also captured in the~~ . Indeed, in current field, in the absence of wind, regional H_s variability results from the wave refraction and the advection of waves action by the current and the group speed (Ardhuin et al., 2017). The doppler-shifted wave frequency by current can also increase the H_s (see introduction of Benetazzo et al. (2013)). Note that current refracts waves such that waves and current can becomes aligned (or opposite). So refraction can trigger a change of mean wave period ~~signal and more noticeable in the perturbed eddy (Fig. 4d,e, f)than in the unperturbed case (Fig. 4a, b, c)~~downstream the refraction areas in the same manner that refraction induce a non-local change of H_s.

For all the variable studied here (Fig.2,3, 4), waves are continuously generated at the left boundary, a solitary incident wave train affect strongly the results presented above, for instance the non-local effect of refraction on the wave field is strongly less pronounced (not shown).

3.2 Ray tracing

In a rotational current field, wave rays are ~~curved~~ bent because of refraction. ~~In a current field the wave elevation variance (or energy)~~ The wave energy spectrum ($E(\sigma,\theta)$) is not conserved ~~, waves and current exchange their own energy, nevertheless~~ in surface currents. Indeed waves and currents exchange energy. Nevertheless wave action (~~$\frac{E(\sigma,\theta)}{\sigma}$~~ $N(\sigma,\theta)$) is conserved ~~. It is~~

~~Instantaneous mean period ($T_{m0,-1}$) for (a,d) T_p=7 , (b,e) 10.3 , and (c,f) 16.6 incident waves. The first line (a,b,c) shows instantaneous field for simulations forced with the unperturbed eddy (Fig.1(a)); the second line (d,e,f) shows the same instantaneous field but for simulations forced with the perturbed eddy (Fig.1(b)). Note that colorbars have different scales for each values of T_p~~

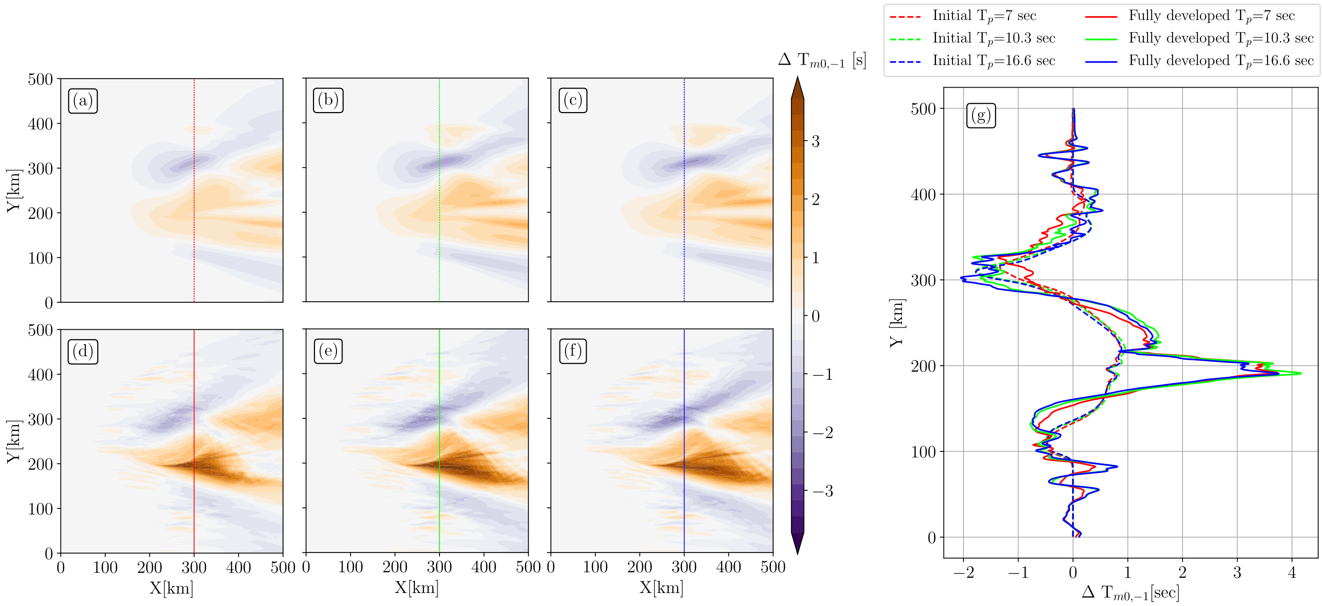

Figure 4. Mean wave period difference ($\Delta T_{m0,-1}$) between simulations forced with and without current ($\Delta T_{m0,-1}$=$T_{m0,-1}$(curr)-$T_{m0,-1}$(Nocurr)). Panels (a,d) show $\Delta T_{m0,-1}$ fields initialized by T_p=7 s wave group. Panels (b,e) show $\Delta T_{m0,-1}$ fields initialized by T_p=10.3 s. Panels (c,f) show $\Delta T_{m0,-1}$ fields initialized by T_p=16.6 s. The first row (a,b,c) shows instantaneous fields for simulations forced with the initial eddy (Fig.1(a,c)); the second row (d,e,f) shows the same fields but for simulations forced with the fully developed eddy (Fig.1(b,d)). Panel (g) shows $\Delta T_{m0,-1}$ along X = 300 km (colored dashed/solid lines in left panels) for all simulations.

~~possible to follow the path along which wave action is conserved thanks to a Monte-Carlo ray tracing (Spencer and Murty, 1962). Refraction seems to be the main process that induce a~~ (Bretherton and Garrett, 1968). In a strong rotational current field, the change of H_s ~~at~~ is mostly driven by refraction from mesoscale and submesoscale ~~(Irvine and Tilley, 1988; Ardhuin et al., 2017; Romero et a~~ ~~.~~

~~In a isolated vortex as described in~~ current (Irvine and Tilley, 1988; Ardhuin et al., 2017; Romero et al., 2020). In the present study, ~~current-induced refraction~~ the isolated vortex modifies waves which results in a strong ~~wave~~ H_s and $T_{m0,-1}$ field inhomogeneity (Fig. 2~~). In the absence of wind and dissipation in a stationary framework, for $\frac{C_g}{u}=\epsilon$ (with $\epsilon \ll 1$), wave refraction can be described through ray equation:~~

$$\cancel{\mathbf{C}_g.\boldsymbol{\nabla}\theta = -\frac{1}{k}\mathbf{n}.\boldsymbol{\nabla}(\mathbf{k}.\mathbf{u}),}$$

~~Refraction is all the more important where waves and currents vectors are perpendicular, given by $\mathbf{n}.\nabla$ term in Eq. (??). In the framework of a monochromatic waves ($\lim_{\sigma\to\sigma_0} E(\sigma)$) and for a prescribed incident direction, refraction can be capture by a~~ , 4). This current-induced refraction is highlighted here thanks to a Monte-Carlo ~~ray tracing method~~ray tracing simulation. The ray-tracing assumes that surface currents are stationary ($\frac{|u|}{C_g} \ll 1$) and that incident waves are monochromatic. In a real ocean, wave field is a superposition of wave ~~train with specific direction and frequency~~trains with specific directions and frequencies, thus ray tracing is only ~~an approximation of the wave kinematic.~~

~~(a,b,c) Ray tracing for waves travelling over an unperturbed eddy with T_p =7 , (a) 10.3 (b), and 16.6 (c) peak period. (d,e,f) same but for waves travelling over a perturbed eddy. Background color shows the surface vorticity, with the same colorscale of Fig 1~~

a very simplified view of how the direction of the waves are modified by the presence of current. Thanks to the ray equation (Eq.3), we expect that refraction is more important where waves and currents vectors are perpendicular (see the $\dot{\theta}$ in Eq.(2) of Ardhuin et al. (2017) or Eq.(17) of Villas Bôas et al. (2020).) Examples of ray-tracing are shown in Fig. 5 in both ~~unperturbed and perturbed eddycases.~~ the initial and fully developed eddy.

The initialized direction is 270° (waves are coming from the ~~west~~ left boundary) and the initial frequencies are the same than the ones discussed above (T_p =7 s, 10.3 s, and 16.6 s peak periods). ~~The~~ We see that the refraction induced by the surface ~~current~~ currents is sensitive to both the nature of underlying current and the frequency (or wavelength) of the incident waves. ~~Indeed, the~~ The radius of curvature of waves rays is larger where the current field is highly rotational (Fig. 5d,e,f) and when simulations are ~~forced~~ initialized with T_p=7 s waves (Fig. 5a,d) ~~(confirmed by theoretical works performed by Kenyon (1971) or Dysthe (2001)).~~

~~In the unperturbed~~ (Kenyon, 1971; Dysthe, 2001). In the initial eddy case, the wave train is refracted both by the eddy's edge (toward the South) and the ~~central part~~ core of the eddy (toward the North) (Fig. 5a,b,c). ~~This~~ It leads to two wave rays focalisation areas ~~(Fig. 5a,b,c)~~downstream the initial eddy. These focalisation areas, or caustics, are slightly shifted zonally toward the ~~east~~ right boundary when the incident wave ~~frequency increases. The number of focalisation areas~~ are longer. The caustic in the upper part of Fig.5 (a,b,c) appears at X=330 km, X=370 km, and X=445 km respectively. In the fully developed field, both mesoscale and submesoscale features refract waves. One can see that the number of caustics increases in the ~~perturbed~~ fully developed eddy with a maximum of ~~convergence zones~~ caustics for T_p= 7 s incident waves ~~, shown in~~ (Fig. 5d). Even if isolated submesoscale eddies have a vorticity comparable with the eddy core ($\frac{\zeta}{f_0}$ ~1.5), they do not refract waves as much as the center structure does. Indeed, if we look at the southernmost submesoscale eddy we see that one wave-ray is deviated of about 30 km from the left boundary to the right boundary whereas one wave ray at the center of the domain is deviated of more than 200 km. The frontal dynamic at the boundary of the main structure of the fully developed eddy induce the strongest wave-ray deviation whereas there scale and their relative vorticity is comparable to submesoscale eddies structures. So the shape of vorticity patterns is key in the intensity of the refraction. One can notice that rays convergent areas are localised where H_s reaches peaks (Fig. 2), specially at the edge of the positive vorticity core. Through realistic numerical studies in strong current fields, Ardhuin et al. (2012) and Kudryavtsev et al. (2017b) showed qualitatively the link between rays caustics and realistic H_s enhancement.

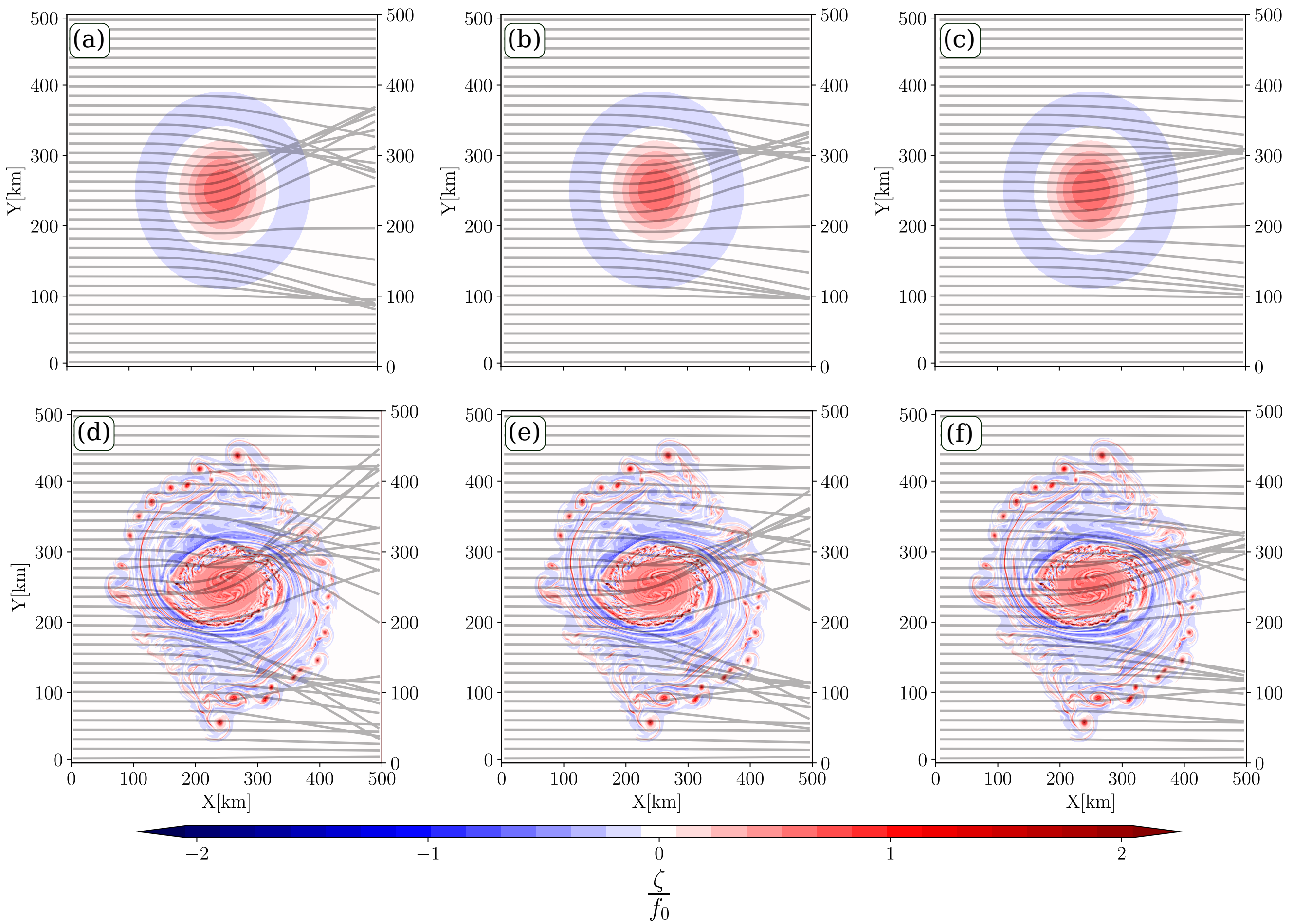

Figure 5. (a,b,c) Ray tracing for waves travelling over the initial eddy with T_p =7 s, (a) 10.3 s (b), and 16.6 s (c) peak period. (d,e,f) same but for waves travelling over the fully developed eddy. The vorticity fields are given in the background.

The strong vorticity field both for ~~unperturbed and perturbed~~ initial and fully developed cyclonic eddy induces a wave rays scattering which can reach a deviation of several hundred kilometers with respect to a propagation without background current~~specially~~ . This deviation is more important for short waves incidence (Fig. 5a,d). ~~These strong scattering~~ The strong wave-scattering can be responsible of the ~~the~~ space-time bias in the ~~waves arrival on the coast forecasts described by Gallet and Young (2014 or Smit and Janssen (2019).~~

~~This~~ forecast of waves arrival (Gallet and Young, 2014; Smit and Janssen, 2019). The ray tracing study ~~highlights the non local effect of current on wave refraction: focalisation can occur even where the surface current is null, thus resulting in wave height enhancement~~ shows that refraction have a local effect on wave direction, strong ray deviations appear where ∇U are strong. However, refraction effects on wave parameters are non-local. We saw that H_s enhancement and wave ray caustics can appear both inside and outside the eddy (Fig.2,5). In other word, strong ∇H_s are not necessarily at strong ∇U locations.

4 Is it possible to reconstruct ~~surface current gradients~~ ∇U *via* the measurement of the ~~wave height gradient~~ ∇ H_s?

~~Surface current gradient module ($\nabla U = \sqrt{\partial_x U^2 + \partial_y U^2}$, $U = \sqrt{u^2+v^2}$) and especially vorticity (ζ)induce a strong wave height gradient (∇H_s) (Villas Bôas et al., 2020; Romero et al., 2020; Marechal and Ardhuin, 2021)~~The ∇H_s at scale between 200 km and $\sim$10 km are associated to the nature of the underlying current (structure and intensity). The current intensity gradients ∇U ($\sqrt{\partial_x U^2 + \partial_y U^2}$) and more specifically the vorticity of the flow, induces refraction resulting in ∇H_s patterns correlated to vorticity patterns (Villas Bôas et al., 2020). Note that both ∇U and ∇H_s are scalars. Assuming ~~Wentzel–Kramers–Brillouin (WKB) approximation~~ that the group speed of waves are much bigger than the intensity of the current velocity,

$$\frac{U}{C_g} << 1, \tag{6}$$

and that waves are ~~generated from a remote storm (no local wind) without breaking, ∇U can be written with respect to∇H_s~~ stationary, the conservation of wave action simplifies to,

$$\frac{H_s}{\sigma} = Cte, \tag{7}$$

leading to the first order approximation:

$$\frac{\nabla H_s \sigma}{(H_s k)} \sim \nabla U. \tag{8}$$

The Eq.(8) ~~such as~~

$$\frac{\nabla H_s \sigma}{(kH_s)} \sim \nabla U$$

shows that ∇H_s is ~~thus function both~~ function of surface current ~~gradient and~~ gradients, wave steepness (kH_s) ~~. The full development is~~ and wave incident frequency. Steps to retrieved the Eq.8 are given in Appendix 1. The motivation of this paragraph is to know if, from high-resolution-wave measurements from filtered altimeter data (Dodet et al., 2020), spectrometers (Hauser et al., 2020) or from optic images (Kudryavtsev et al., 2017b), the nature of the flow can be estimated. Today's surface currents measurements from Sea-Level-Anomaly can capture eddy with a shape similar to Fig.1a,c (if their lifetime are sufficiently long according to the revisiting-time of altimeters). However eddy with a more realistic shape (Fig.1b,d) are very poorly captured (see section 5.2 of de Marez et al. (2020b)). Thanks to our numerical results we will test the validity of Eq.8 in the case of fully developed eddy. The final aim is to know if the nature of the flow can be estimated by inverting high resolution H_s,σ (or k) measurements. Right and left hand sides of Eq. (8) are shown in Fig. 6 ~~in the perturbed~~ (a,b) in the fully

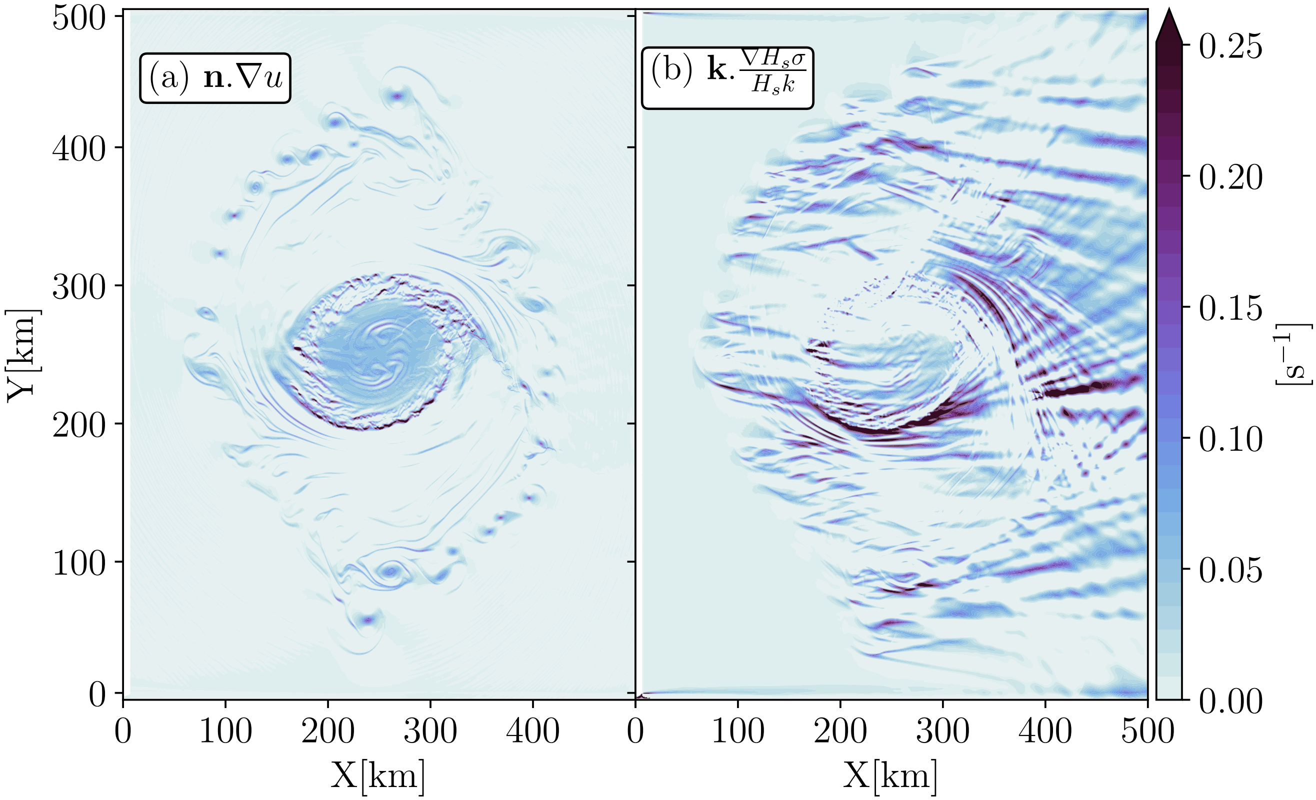

Figure 6. (a) Surface current gradients (∇u) projected perpendicular to the peak wave direction vector, *i.e.* the right hand side of Eq. (8) and (b) normalized wave height gradient ($\frac{\nabla H_s \sigma}{H_s k}$) projected in the peak wave direction vector, *i.e.* the left hand side of Eq. (8), both for the fully developed eddy. These instantaneous fields are for simulation initialized with T_p = 7 s.

developed eddy case, for incident waves at T_p=7 s. ~~Both~~ ∇H_s and ∇U have been projected along and perpendicular to the wave peak direction respectively. Both terms of Eq. (8) are of the same order of magnitude with values slightly higher for the $\frac{\nabla H_s \sigma}{(k H_s)}$ field (Fig. 6b). ∇U shows rounded structures (Fig. 6a) whereas ∇H_s field shows more elongated-horizontal ~~, typical structures of current-induced refraction (Villas Bôas et al., 2020; de Souza et al., 2021). Nevertheless~~structures aligned with the initial wave direction (270°). From X=0 km to X=250 km, normalized ∇H_s patterns are aligned with the incident wave directions, downstream X=250 km patterns follow the rays trajectories shown in Fig.5d. Apart from the difference of shape, both fields are matching both at mesoscale (the central eddy) and at smaller scale (submesoscale eddies around the ~~principal core of the~~ ellipsoidal eddy) from X=0 km to X=250 km. ∇U exhibits fronts at the boundary of the central eddy also captured by the normalized ∇H_s field. Inside the central ellipsoidal eddy (between Y=200 km and 300 km), ∇U shows a ~~quite~~ smooth and homogeneous field which is captured in Fig. 6b only between Y=200 km and 250 km. Reader can also see discrepancies between the two fields, between the central eddy and the submesoscales eddies, where sharp ∇H_s are shown whereas ∇U are

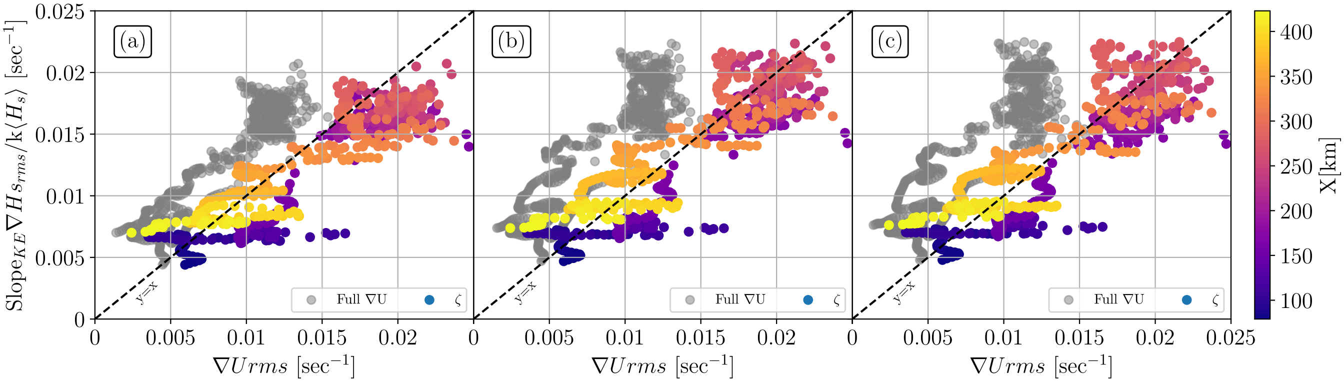

Figure 7. Scatter plot of the normalized root-mean-square of significant wave height gradients as a function of root-mean-square surface current gradients. Colored points are the scatter plot for the vorticity component of the surface current gradients and grey points for the full surface current gradient (diverging component + rotational component). One point correspond to the root-mean-square of the two quantities for constant X, the value of X is given as colorscale. $<\mathrm{H}_s>$ is the average value of the significant wave height when simulations reach the stationnary state. Panel (a), (b) and (c) are for simulations forced with the fully developed eddy initialized with T_p=7 sec, T_p=10.3 sec, and T_p=16.6 sec respectively.

very smooth. Downstream the eddy even if ∇U is null (Fig.6a)~~whereas~~, normalized $\nabla \mathrm{H}_s$ are very sharp (Fig.6b~~presents ∇H_s stripes.~~). The non-local effect of current gradients on the H_s is thus well highlighted through this diagnostic.

The analysis of Fig. 6b shows that the wave ~~model captures~~ simulations capture surface currents gradient in the first half of the domain, without any information on surface current. The ~~sensibility of wave field gradient to~~ inversion of the ~~spectral width (σ_f~~ $\nabla \mathrm{H}_s$ to infer the underlying surface currents seemed to be promising, however both the non-local effect of currents on waves and the initial incidence direction (resulting in a privileged direction of $\nabla \mathrm{H}_s$ patterns) show that the phase of current gradient is hardly reproduced in most of the part of the domain. It proved some limitations in the ∇ H_s inversion to infer ∇ U. To better describe the robustness of the formula given in Eq. 8 we proposed a scatter plot of the root-mean-square (rms) of the ~~incident wave packet have been tested, the results shown~~left hand side as a function of the rms of the right hand side of Eq.(8). Results are given in Fig.7. As proved numerically by Villas Bôas et al. (2020), we have multiplied the left-hand-side of Eq.(8 by 3 which is the absolute value of the slope of the Kinertic Energy spectrum of the fully developed eddy. A point in Fig.7 is the rms of the normalized $\nabla \mathrm{H}_s$ and of the ∇U at fixed distance from the left boundary. The diagnostics have been done both for the full gradients of the surface currents (divergence and vorticity) and only for the vorticity component. Villas Bôas et al. (2020) proved that $\nabla \mathrm{H}_s$ is strongly proportional to the vorticity component of the flow (see their Fig.12), we wanted to show here the effect of the divergence on the proportionality between ∇H_s and ∇U. The divergence component of the surface gradients is one order of magnitude smaller than the rotationnal one (not shown.) We do not focus on the gradients for X<79 km and X>423 km because ∇U are null. Thanks to a linear regression between points in Fig.~~8b are not affected by this modification in the wave model~~7, we verified that ∇H_s and ∇U (vorticity) are strongly proportional. Slope are equal to 1.13 (0.72), 1.20 (0.8), and 1.17 (0.8) for simulations initialized with T_p=7 sec, T_p=10.3 sec, and T_p=16.6 sec. However the coefficient of determination

(R2) is negative for the rms of the full ∇U with respect to ∇H_s meaning that the linear relation between ∇H_s and ∇U is not verified. When the rms of ∇H_s is compare to the rms of ζ we confirm the results of Villas Bôas et al. (2020) between X=79 km and X=423 km with R2 varying within 0.67 and 0.75 for all initializations.

Where oceanic eddy ~~became~~ becomes unstable spontaneously due to horizontal sheared current structures (barotropic instabilities) or vertical buoyancy gradient (baroclinic instabilities, mixed layer instabilities), the resulting ocean surface ~~provide~~ shows specific ∇U features. ~~Certain of these structures are well captured by the normalized ∇H_s field. Oceanic meso- and submesoscale instabilities can induce mixing, vertical movements or water masses trapping which could be now approached only thanks to an investigation of ∇H_s field. Regional ∇H_s field are possibly recoverable at very high resolution thanks to remote sensing imagery as optical techniques (Kudryavtsev et al., 2017a).~~

~~These results point out the promising opportunities to invert wave gradient properties to retrieve the underlying surface current gradient at high resolution , specially at scales where altimeters are unable to reconstruct~~Thanks to wave numerical experiments we were able to observe ∇H_s structures which are similar to the structures of ∇U and more specially to the vorticity component of ∇U. The amplitude of the two gradients are comparable if we know the nature of the incident waves. It seems promising to invert the waves signal to infer the underlying vorticity field and, perhaps, the instabilities that created such structures (according to the shape and the size of ∇ H_s). Optical instruments have shown there robustness to retrieve both the phase and the amplitude of the waves field at an unprecedented spatial resolution ($\sim$ 10 m) in a very wide swath (Kudryavtsev et al., 2017b)). The use of such instrument seems to be a good candidate to capture very small-scale current features by inverting wave characteristics as shown in the fully developed eddy. Nevertheless there is one drawback, and not least, the non-local effects of current on H_s which make emerge ∇H_s where current is null.

~~(a) Surface current gradient (∇u) projected perpendicular to the peak wave direction vector, *i.e.* the right hand side of Eq. (8) and (b) normalized wave height gradient ($\frac{\nabla H_s \sigma}{H_s k}$) projected in the peak wave direction vector, *i.e.* the left hand side of Eq. (8), both for the perturbed eddy case. This instantaneous field is for simulation initialized with T_p = 7 .~~

Measuring surface currents from space is a very challenging purpose since past decades (Villas Bôas et al., 2019). Altimetry has proved its robustness to ~~retrieve surface current~~ capture surface geostrophic current at global scale by measuring the ~~dynamical ocean height at a resolution of several hundred kilometers (Rio et al., 2014; Ballarotta et al., 2019). The benefits of this method is mainly the global coverage of the ocean surface in a dozen of days by combining several altimeters missions. Nevertheless, although altimeters sample ocean surface every ∼10 , the accumulation of noise along altimeter track induces a loss of resolution in~~ along track Sea-Level-Anomaly from multiple altimeter missions. The effective resolution of the ~~surface current retrieval~~current depends principally on the number of satellites. The resolution of global map of surface currents derived from altimetry has been calculated and show a mean effective resolution higher than 250 km at mid-latitudes and more than 600 km in the equatorial band (Rio et al., 2014; Ballarotta et al., 2019). Even if mesoscale eddies are observable from space (Chelton et al., 2011), surface dynamics at smaller scales are ~~drawn in the noise signal~~not captured by present altimeter products. As an example we can cite the small oceanic features in the fully developed eddy (see section 5.2 section of de Marez et al. (2020b)). This reality has highlighted the necessity to measure surface currents at higher resolution triggering the emergence of new satellite missions based on innovative measurements ~~method (Ardhuin et al., 2018; Morrow et al., 2019; Ardhuin et al., 2021).~~

~~In term of wave-current interactions, as current affects waves principally at scales smaller than 200 (Ardhuin et al., 2017; Villas Bôas et al., , waves models forced with currents derived from altimetry do not reproduce realistic ∇H_s (Marechal and Ardhuin, 2021) or wave breaking statistic (Romero et al., 2017, 2020). This is all the more true in boundary currents where mesoscale and submesoscale are ubiquitous (Rocha et al., 2016; Mensa et al., 2013). The small scale dynamic present in the perturbed eddy field used in this study is not captured by potential altimeter measurements (see discussion in de Marez et al. (2020b)).~~ methods (Ardhuin et al., 2018; Morrow et al., 2019; Ardhuin et al., 2021).

~~In this study, we showed that a realistic eddy fieldinduces inhomogeneities~~

5 Effects on broader banded incident spectra and nonlinear wave-wave interactions on wave-current interactions

5.1 New model setup

In the previous analysis the incident waves have been simulated via wave spectra gaussian in frequency with a frequency spreading (σ_f) equal to 0.03 Hz. For time scale much larger than the wave period and a gaussian surface, nonlinear wave-wave interaction trigger a change of the wave energy in the wave field Hasselmann (1962). Here we wanted to quantify the effects of nonlinear wave-wave interactions on the wave parameter gradients in a current field. To study the cross-spectral energy flux between frequencies we activated the nonlinear source term (S_{nl}). The right hand side of Eq.(1) was thus not equal to 0 any more but to S_{nl}. Because simulations initialized with very narrow banded spectrum do not show a clear difference between simulations with and without S_{nl} (not shown), we extended the frequency spreading of the incident wave trains to σ_f=0.1 Hz. For sufficiently steep waves, nonlinear wave-wave interactions redistribute wave energy between frequencies over the spectrum which strongly modifies the shape of the spectrum (Komen et al., 1984). As ∇H_s is function of the wave steepness (kH_s, Fig.8) we expected that nonlinear wave-wave interactions would have an impact on the intensity of the wave parameters gradients. Nonlinear wave-wave interactions have been modeled using the discrete interaction approximation (Hasselmann et al., 1985) . The wave simulation has been run during a sufficiently long time to capture the long term effect of nonlinear wave-wave interactions on the wave parameters. Wave simulation has been performed only for 7 sec incident waves over the fully developed eddy field. This section is a simple introduction of how both wave-wave interactions and wave-current interactions could induced inhomogeneity in the wave field still in a very idealized framework. Further investigation wil be required.

5.2 Results

For a given wave parameter (H_s or $T_{m0,-1}$), the relative difference has been computed between simulations where nonlinear source term was activated and desactivated (Eq.9),

$$\Delta X = \frac{X_{S_{nl}} - X_{noS_{nl}}}{X_{noS_{nl}}} \times 100. \tag{9}$$

The nonlinear wave-wave interactions have a large effect on the spatial gradient of wave parameters studied before, H_s are globally enhanced whereas $T_{m0,-1}$ are decreased (Fig.8). The spatial variability of the H_s can reach +80% for X>250 km at Y$\sim$200 km when S_{nl} is activated. It has been shown that at the same location, wave-current interactions alone showed a strong decrease of H_s (Fig.2). One can see also that simulation with wave-wave interactions enhance the H_s at the periphery of the eddy core of the fully developed eddy, in the submesoscale eddy field area. Globally, we see that H_s increases where wave-currents interactions have decrease the H_s. One can see that areas where enhancement of H_s have been noticed in Fig.2 are not modified in Fig.8a or only slightly. Please notice that we cannot compare quantitatively Fig.8a and Fig.2d because the incident waves have a different spreading in frequency. Nonlinear wave-wave interactions also highlight a change in the $T_{m0,-1}$ field. $\Delta T_{m0,-1}$ shows the opposite spatial variation of Δ H_s. Indeed, where Δ H_s were (strongly) positive, $\Delta T_{m0,-1}$ is (strongly) negative and vice versa. A transects at X=300 km show the values of H_s and $T_{m0,-1}$ along the vertical (Fig.8c,d). One can see that ∇ H_s are globally reduced due to nonlinear wave-wave interaction specially in the core of the central eddy (Y between 200 km and 350 km). At location of submesoscale eddies, ∇H_s are also sharper for simulation without S_{nl} but the difference between the two parametrizations are less pronounced. ∇ $T_{m0,-1}$ show a much more striking difference between simulations with and without nonlinear wave-wave interactions,. ∇ $T_{m0,-1}$ are the most pronounced also in the core of the eddy where wave period can reach a 4 sec difference whereas simulation with S_{nl} reveal only a change of 2 sec. Whether for H_s or $T_{m0,-1}$, in current field, wave-wave interactions have the tendency to decrease spatial gradients of the wave parameters triggered by wave-current interactions. Here the choice of the parametrization of the nonlinear wave-wave interactions was arbitrary (Hasselmann et al., 1985), it would be interesting to expand this study to other parametrizations of S_{nl} to better describe how nonlinear wave-wave processes modify regional wave parameter gradients.

6 Conclusion and perspectives

~~A new study of wave-current interactions have been investigated in a highly rotational isolated vortex~~In this paper, we studied numerically the effect of an isolated composite cyclonic eddy on the wave properties. High resolution wave simulations have been forced by a composite eddy reconstructed from in-situ measurements in the Arabian Sea. The wave model has been forced on the one hand by the initial eddy field (gaussian shape) and, on the other hand, by the fully developed eddy resulting from the destabilization within the composite eddy. Waves have been simulated by the use of a third generation phase averaged spectral model initialized with narrow wave spectra centered at different ~~frequency~~ frequencies (T_p =7 , 10.3, and 16.6 s). Although wave scattering by an oceanic vortex has already been studied in ~~the past (Mathiesen, 1987; White and Fornberg, 1998; Gallet and Young, 2~~ former papers (Mapp et al., 1985; White and Fornberg, 1998; Gallet and Young, 2014), this study completes studies performed in the past with *(1)* a description of the evolution of the wave bulk parameters as significant wave height and mean wave period inside and outside the isolated vortex, and *(2)* the investigation of how a ~~realistic and perturbed~~ fully developed eddy (that really occur in a real ocean) ~~induces variability in~~ modify the wave field. Both wave ~~dynamics~~ dynamic and kinematics are changed by the presence of an underlying current. These changes are ~~all the more pronounced~~ more pronounced where the underlying current gradients are strong and when incident waves are ~~shorts and where the underlying current is highly energetic within a large band of scales.~~ short. This is coherent with the studies of Kenyon (1971); Dysthe (2001). As multi-scale dynamic eddies are certainly more realistic in the ocean than gaussian eddies, former studies of interaction between wave and gaussian

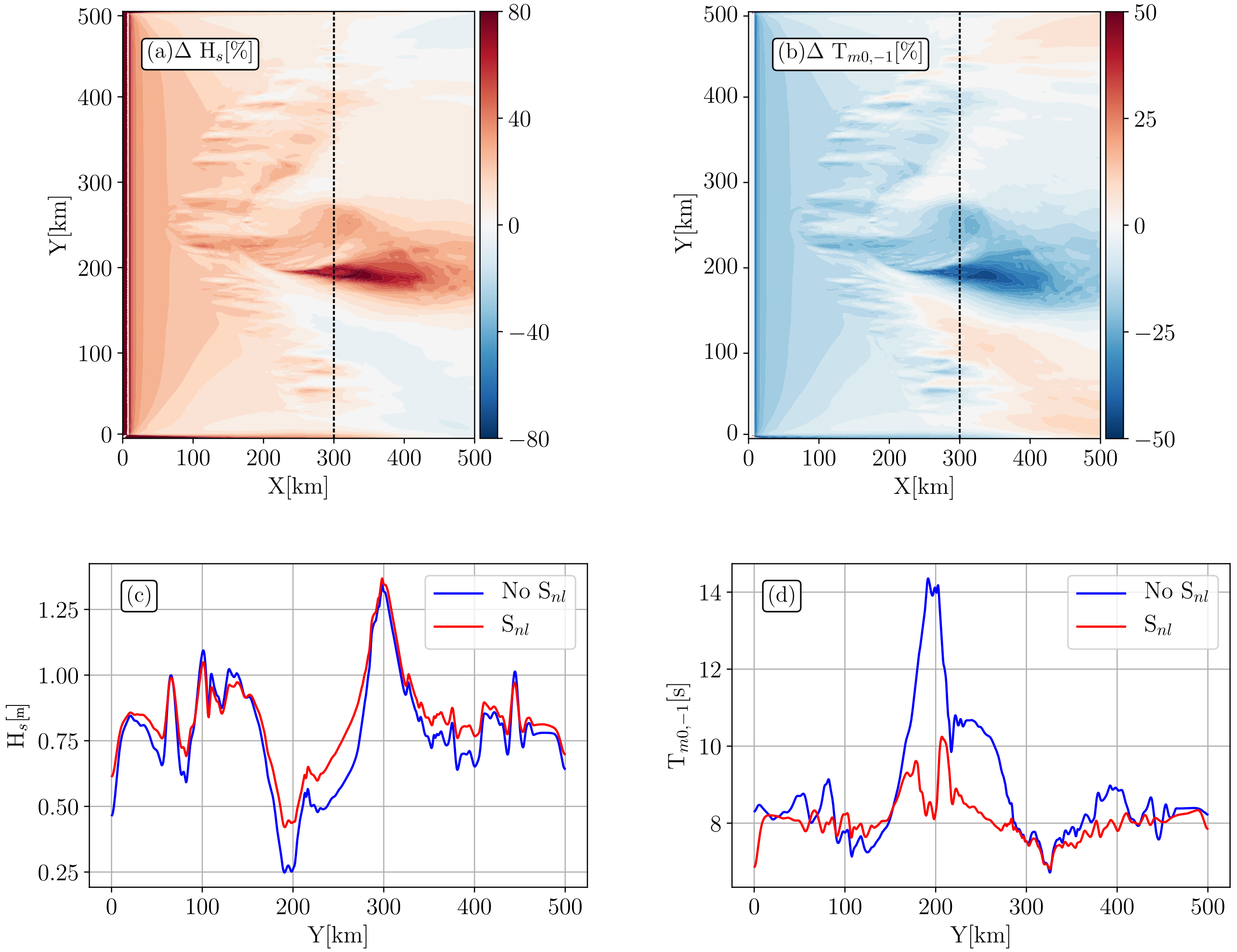

Figure 8. Model difference between solutions with and without nonlinear wave-wave interactions. Panel (a) and (b) show the relative difference in percent of the significant wave height and the mean wave period. Panel (c) and (d) show a transect at X=300 km for simulations without (solid blue line) and with (solid red line) nonlinear source term (S_{nl}) for H_s and $T_{m0,-1}$ respectively

eddy underestimate wave refraction, extreme significant wave heights but also wave steepness because surface currents also induce a non negligible change of wave period (wavelength). Those underestimations can have a large impact on the waves forecast but also on the source of noise induced by waves in the ocean level measurements by altimeters. Tran et al. (2010) proposed to combined altimeter measurements and wave simulations in order to develop a global sea-state bias model. Thanks to the period provided by wave model (only forced by wind) authors showed the possibility to reduce the error budget of $\sim$7.5%. However they parametrized their wave model on a too much coarse grid ($1° \times 1°$) without taken into account current forcing. As we proved here, short-scale currents induce large changes of wave period at regional scale (smaller than wind scale patterns). Indeed, even in a very idealized eddy, $\Delta T_{m0,-1}$ oscillates within 1 sec (Fig. 4a-c) and reaches $\sim$3 sec for a more realistic eddy pattern (Fig. 4a-c). Redo the same work of Tran et al. (2010) at higher resolution with current sufficiently resolved (Marechal and Ardhuin, 2021) would be benefit to improved their sea-states bias model at regional scale.

Under the WKB approximation and in the geometric theory framework, the significant wave height ~~gradient field normalized by wave frequency of the incident waves~~ gradients normalized by the incident wave frequency has been described as a function of the surface current ~~gradient~~gradients. Besides a good coherence in ~~order~~ terms of magnitude between the two quantities, structures of significant wave height gradient are very sensitive to the underlying surface current. ~~Measurements of sea surface height~~ We know that measurements of sea level anomaly from space are able to monitoring surface currents at global scale ~~until~~ with a wavelength resolution of several hundreds kilometers in a ice-free areas (Villas Bôas et al., 2019). All the surface ~~dynamic~~ dynamics at smaller scales cannot be ~~retrieved by the used of a constellations of traditional~~ captured by altimeters whereas a lot of oceanic processes occur at those scales (from 1-100 km). This manuscript have shown the possibility to ~~invert~~ infer the vorticity of the eddy field from the inhomogeneity in the waves field~~to retrieved surface current gradients and thus approach the small scale~~ , as proposed in Villas Bôas et al. (2020). Infer vorticity patterns could allow to capture the small-scale processes (vertical movements, mixing, shear flows...) without measurement of surface currents.

~~Finally, investigations of fully couple simulations (atmosphere-waves-ocean) could be performed to investigate how the realistic vortex is modified by the wave-induced Stokes drift or how potential breaking events induce by the current modify the air entrainment and thus the turbulence in the atmospheric boundary layers.~~

Nevertheless, this inversion could not works in the vicinity of a strong ∇U field because waves keep in memory the effect of upstream currents resulting in a regional inhomogeneity in the wave field even if the current gradients are null. As measuring surface currents both at global scale and high resolution being a present challenge for the oceanographic community, different strategy have been imagined. Infer ∇U from ∇H_s seemed to be a good strategy, but because the wave-current coupled system is too much complex, much more than the one proposed here, assumption proposed in this manuscript are hardly satisfied in nature. Moreover, even in a very simplified framework as proposed here, the wave inversion is, at the best, only partial. So one possible solution would be a direct measurement of surface currents from space as proposed in Ardhuin et al. (2018).

Data availability. The cyclonic vortex field is available at https://data.mendeley.com/datasets/bwkctkk5bn/1.

References

Ardhuin, F., Roland, A., Dumas, F., Bennis, A.-C., Sentchev, A., Forget, P., Wolf, J., Girard, F., Osuna, P., and Benoit, M.: Numerical wave modeling in conditions with strong currents: Dissipation, refraction, and relative wind, Journal of Physical Oceanography, 42, 2101–2120, 2012.

Ardhuin, F., Rascle, N., Chapron, B., Gula, J., Molemaker, J., Gille, S. T., Menemenlis, D., and Rocha, C.: Small scale currents have large effects on wind wave heights, J. Geophys. Res., 122, 4500–4517, https://doi.org/10.1002/2016JC012413, 2017.

Ardhuin, F., Aksenov, Y., Benetazzo, A., Bertino, L., Brandt, P., Caubet, E., Chapron, B., Collard, F., Cravatte, S., Dias, F., Dibarboure, G., Gaultier, L., Johannessen, J., Korosov, A., Manucharyan, G., Menemenlis, D., Menendez, M., Monnier, G., Mouche, A., Nouguier, F., Nurser, G., Rampal, P., Reniers, A., Rodriguez, E., Stopa, J., Tison, C., Tissier, M., Ubelmann, C., van Sebille, E., Vialard, J., and Xie, J.: Measuring currents, ice drift, and waves from space: the Sea Surface KInematics Multiscale monitoring (SKIM) concept, Ocean Sci., 14, 337–354, https://doi.org/10.5194/os-2017-65, 2018.

Ardhuin, F., Alday Gonzalez, M. F., and Yurovskaya, M.: Total Surface Current Vector and Shear from a Sequence of Satellite images: Effect of Waves in Opposite Directions, Earth and Space Science Open Archive, 2021.

Ballarotta, M., Ubelmann, C., Pujol, M.-I., Taburet, G., Fournier, F., Legeais, J.-F., Faugere, Y., Delepoulle, A., Chelton, D., Dibarboure, G., and Picot, N.: On the resolutions of ocean altimetry maps, Ocean Science Discussions, https://doi.org/10.5194/os-2018-156, 2019.

Benetazzo, A., Carniel, S., Sclavo, M., and Bergamasco, A.: Wave–current interaction: Effect on the wave field in a semi-enclosed basin, Ocean Modelling, 70, 152–165, 2013.

Bretherton, F. P. and Garrett, C. J. R.: Wavetrains in inhomogeneous moving media, Proceedings of the Royal Society of London. Series A. Mathematical and Physical Sciences, 302, 529–554, 1968.

Bruch, W., Piazzola, J., Branger, H., van Eijk, A. M., Luneau, C., Bourras, D., and Tedeschi, G.: Sea-Spray-Generation Dependence on Wind and Wave Combinations: A Laboratory Study, Boundary-Layer Meteorology, pp. 1–29, 2021.

Cavaleri, L., Fox-Kemper, B., and Hemer, M.: Wind Waves in the Coupled Climate System, Bull. Amer. Meteorol. Soc., 78, 1651–1661, 2012.

Chelton, D. B., deSzoeke, R. A., Schlax, M. G., El Naggar, K., and Siwertz, N.: Geographical Variability of the First Baroclinic Rossby Radius of Deformation, Journal of Physical Oceanography, 28, 433–460, https://doi.org/10.1175/1520-0485(1998)028<0433:GVOTFB>2.0.CO;2, 1998.

Chelton, D. B., Schlax, M. G., Samelson, R. M., and de Szoeke, R. A.: Global observations of large oceanic eddies, Geophysical Research Letters, 34, https://doi.org/10.1029/2007GL030812, 2007.

Chelton, D. B., Schlax, M. G., and Samelson, R. M.: Global observations of nonlinear mesoscale eddies, Progress in Oceanography, 91, 167–216, https://doi.org/10.1016/j.pocean.2011.01.002, 2011.

de Marez, C., L'Hégaret, P., Morvan, M., and Carton, X.: On the 3D structure of eddies in the Arabian Sea, Deep Sea Research Part I: Oceanographic Research Papers, 150, 103 057, https://doi.org/10.1016/j.dsr.2019.06.003, 2019.

de Marez, C., Carton, X., Corréard, S., L'Hégaret, P., and Morvan, M.: Observations of a deep submesoscale cyclonic vortex in the Arabian Sea, Geophysical Research Letters, 47, e2020GL087 881, 2020a.

de Marez, C., Meunier, T., Morvan, M., L'Hégaret, P., and Carton, X.: Study of the stability of a large realistic cyclonic eddy, Ocean Modelling, 146, 101 540, https://doi.org/10.1016/j.ocemod.2019.101540, 2020b.

de Souza, J. M. A. C., Couto, P., Soutelino, R., and Roughan, M.: Evaluation of four global ocean reanalysis products for New Zealand waters–A guide for regional ocean modelling, New Zealand Journal of Marine and Freshwater Research, 55, 132–155, 2021.

Dodet, G., Piolle, J.-F., Quilfen, Y., Abdalla, S., Accensi, M., Ardhuin, F., Ash, E., Bidlot, J.-R., Gommenginger, C., Marechal, G., Passaro, M., Quartly, G., Stopa, J., Timmermans, B., Young, I., Cipollini, P., and Donlon, C.: The Sea State CCI dataset v1: towards a sea state climate data record based on satellite observations, Earth System Sci. Data, 12, 1929–1951, https://doi.org/10.5194/essd-12-1929-2020, 2020.

Dysthe, K. B.: Refraction of gravity waves by weak current gradients, J. Fluid Mech., 442, 157–159, 2001.

Fu, L.-L. and Glazman, R.: The effect of the degree of wave development on the sea state bias in radar altimetry measurement, Journal of Geophysical Research: Oceans, 96, 829–834, 1991.

Gallet, B. and Young, W. R.: Refraction of swell by surface currents, J. Mar. Res., 72, 105–126, https://doi.org/10.1357/002224014813758959, 2014.

Gula, J., Molemaker, M., and McWilliams, J.: Topographic vorticity generation, submesoscale instability and vortex street formation in the Gulf Stream, Geophysical Research Letters, 42, 4054–4062, 2015a.

Gula, J., Molemaker, M. J., and Mcwilliams, J. C.: Gulf Stream Dynamics along the Southeastern U.S. Seaboard, J. Phys. Oceanogr., 45, 690–715, 2015b.

Hasselmann, K.: On the non-linear energy transfer in a gravity-wave spectrum Part 1. General theory, Journal of Fluid Mechanics, 12, 481–500, 1962.

Hasselmann, K., Chapron, B., Aouf, L., Ardhuin, F., Collard, F., Engen, G., Hasselmann, S., Heimbach, P., Janssen, P., Johnsen, H., Krogstad, H., Lehner, S., Li, J.-G., Li, X.-M., Rosenthal, W., and Schulz-Stellenfleth, J.: The ERS SAR Wave Mode: a breakthrough in global ocean wave observations, in: ERS Missions: 20 Years of Observing Earth, pp. 165–198, European Space Agency, Noordwijk, The Netherlands, 2012.

Hasselmann, S., Hasselmann, K., Allender, J., and Barnett, T.: Computations and parameterizations of the nonlinear energy transfer in a gravity-wave specturm. Part II: Parameterizations of the nonlinear energy transfer for application in wave models, Journal of Physical Oceanography, 15, 1378–1391, 1985.

Hauser, D., Tourain, C., Hermozo, L., Alraddawi, D., Aouf, L., Chapron, B., Dalphinet, A., Delaye, L., Dalila, M., Dormy, E., et al.: New observations from the SWIM radar on-board CFOSAT: Instrument validation and ocean wave measurement assessment, IEEE Transactions on Geoscience and Remote Sensing, 59, 5–26, 2020.

Holthuijsen, L. and Tolman, H.: Effects of the Gulf Stream on ocean waves, Journal of Geophysical Research: Oceans, 96, 12 755–12 771, 1991.

Hua, B. L., Ménesguen, C., Le Gentil, S., Schopp, R., Marsset, B., and Aiki, H.: Layering and turbulence surrounding an anticyclonic oceanic vortex: In situ observations and quasi-geostrophic numerical simulations, Journal of Fluid Mechanics, 731, 418–442, 2013.

Huang, N. E., Chen, D. T., Tung, C.-C., and Smith, J. R.: Interactions between steady won-uniform currents and gravity waves with applications for current measurements, Journal of Physical Oceanography, 2, 420–431, 1972.

Irvine, D. E. and Tilley, D. G.: Ocean wave directional spectra and wave-current interaction in the Agulhas from the shuttle imaging radar-B synthetic aperture radar, J. Geophys. Res., 93, 15 389–15 401, 1988.

Kenyon, K. E.: Wave refraction in Ocean Current, Deep-Sea Res., 18, 1971.

Kirby, J. T. and Chen, T.-M.: Surface waves on vertically sheared flows: approximate dispersion relations, Journal of Geophysical Research: Oceans, 94, 1013–1027, 1989.

Komen, G., Hasselmann, S., and Hasselmann, K.: On the existence of a fully developed wind-sea spectrum, Journal of physical oceanography, 14, 1271–1285, 1984.

Kudryavtsev, V., Yurovskaya, M., Chapron, B., Collard, F., and Donlon, C.: Sun glitter Imagery of Surface Waves. Part 1: Directional spectrum retrieval and validation, J. Geophys. Res., 122, https://doi.org/10.1002/2016JC012425, 2017a.

Kudryavtsev, V., Yurovskaya, M., Chapron, B., Collard, F., and Donlon, C.: Sun glitter Imagery of Surface Waves. Part 2: Waves Transformation on Ocean Currents, J. Geophys. Res., 122, https://doi.org/10.1002/2016JC012426, 2017b.

Lavrenov, I.: The wave energy concentration at the Agulhas current off South Africa, Natural hazards, 17, 117–127, 1998.

Le Vu, B., Stegner, A., and Arsouze, T.: Angular Momentum Eddy Detection and Tracking Algorithm (AMEDA) and Its Application to Coastal Eddy Formation, Journal of Atmospheric and Oceanic Technology, 35, 739–762, https://doi.org/10.1175/JTECH-D-17-0010.1, 2018.

Lévy, M., Franks, P. J. S., and Smith, K. S.: The role of submesoscale currents in structuring marine ecosystems, Nature Communications, 9, 4758, https://doi.org/10.1038/s41467-018-07059-3, 2018.

Mapp, G. R., Welch, C. S., and Munday, J. C.: Wave refraction by warm core rings, Journal of Geophysical Research: Oceans, 90, 7153–7162, 1985.

Marechal, G. and Ardhuin, F.: Surface Currents and Significant Wave Height Gradients: Matching Numerical Models and High-Resolution Altimeter Wave Heights in the Agulhas Current Region, Journal of Geophysical Research: Oceans, 126, e2020JC016 564, 2021.

Mathiesen, M.: Wave refraction by a current whirl, J. Geophys. Res., 92, 3905–3912, 1987.

McWilliams, J. C.: Submesoscale currents in the ocean, 427, 20160 117, https://doi.org/10.1098/rspa.2016.0117, 2016.

Mei, C. C.: Applied dynamics of ocean surface waves, World Scientific, Singapore, second edn., 740 p., 1989.

Mensa, J. A., Garraffo, Z., Griffa, A., Özgökmen, T. M., Haza, A., and Veneziani, M.: Seasonality of the submesoscale dynamics in the Gulf Stream region, Ocean Dynamics, 63, 923–941, 2013.

Monahan, E. C., Spiel, D. E., and Davidson, K. L.: A model of marine aerosol generation via whitecaps and wave disruption, in: Oceanic whitecaps, pp. 167–174, Springer, 1986.

Morrow, R., Fu, L.-L., Ardhuin, F., Benkiran, M., Chapron, B., Cosme, E., D?Ovidio, F., Farrar, J. T., Gille, S. T., Lapeyre, G., Traon, P.-Y. L., Pascual, A., Ponte, A., Qiu, B., Rascle, N., Ubelmann, C., Wang, J., and Zaron, E. D.: Global observations of fine-scale ocean surface topography with the Surface Water and Ocean Topography (SWOT) Mission, 6, 232, https://doi.org/10.3389/fmars.2019.00232, 2019.

Phillips, O. M.: The dynamics of the upper ocean, Cambridge University Press, London, 336 p., 1977.

Quilfen, Y. and Chapron, B.: Ocean Surface Wave-Current Signatures From Satellite Altimeter Measurements, Geophys. Res. Lett., 216, 253–261, https://doi.org/10.1029/2018GL081029, 2019.

Quilfen, Y., Yurovskaya, M., Chapron, B., and Ardhuin, F.: Storm waves sharpening in the Agulhas current: satellite observations and modeling, Remote Sens. Environ., 216, 561–571, https://doi.org/10.1016/j.rse.2018.07.020, 2018.

Rio, M.-H., Mulet, S., and Picot, N.: Beyond GOCE for the ocean circulation estimate: Synergetic use of altimetry, gravimetry, and in situ data provides new insight into geostrophic and Ekman currents, Geophys. Res. Lett., 41, 8918–8925, https://doi.org/10.1002/2014GL061773, 2014.

Rocha, C. B., Chereskin, T. K., and Gille, S. T.: Mesoscale to Submesoscale Wavenumber Spectra in Drake Passage, J. Phys. Oceanogr., 46, 601–620, https://doi.org/10.1175/JPO-D-15-0087.1, 2016.

Romero, L., Lenain, L., and Melville, W. K.: Observations of Surface Wave–Current Interaction, J. Phys. Oceanogr., 47, 615–632, https://doi.org/10.1175/JPO-D-16-0108.1, 2017.

Romero, L., Hypolite, D., and McWilliams, J. C.: Submesoscale current effects on surface waves, Ocean Modelling, 153, 101 662, 2020.

Sandwell, D. T. and Smith, W. H.: Retracking ERS-1 altimeter waveforms for optimal gravity field recovery, Geophysical Journal International, 163, 79–89, 2005.

Shchepetkin, A. F. and McWilliams, J. C.: The regional oceanic modeling system (ROMS): a split-explicit, free-surface, topography-following-coordinate oceanic model, Ocean Modelling, 9, 347–404, https://doi.org/10.1016/j.ocemod.2004.08.002, 2005.

Shchepetkin, A. F. and McWilliams, J. C.: Accurate Boussinesq oceanic modeling with a practical, "Stiffened" Equation of State, Ocean Modelling, 38, 41–70, https://doi.org/10.1016/j.ocemod.2011.01.010, 2011.

Sheres, D., Kenyon, K. E., Bernstein, R. L., and Beardsley, R. C.: Large horizontal surface velocity shears in the ocean obtained from images of refracting swell and in situ moored current data, Journal of Geophysical Research: Oceans, 90, 4943–4950, 1985.

Smit, P. B. and Janssen, T. T.: Swell propagation through submesoscale turbulence, Journal of Physical Oceanography, 49, 2615–2630, 2019.

Spencer, G. and Murty, M.: General ray-tracing procedure, JOSA, 52, 672–678, 1962.

Tedesco, P., Gula, J., Ménesguen, C., Penven, P., and Krug, M.: Generation of submesoscale frontal eddies in the Agulhas Current, Journal of Geophysical Research: Oceans, 124, 7606–7625, 2019.

The WAVEWATCH III® Development Group: User manual and system documentation of WAVEWATCH III ® version 5.16, Tech. Note 329, NOAA/NWS/NCEP/MMAB, College Park, MD, USA, 326 pp. + Appendices, 2016.

Tran, N., Vandemark, D., Labroue, S., Feng, H., Chapron, B., Tolman, H. L., Lambin, J., and Picot, N.: The sea state bias in altimeter sea level estimates determined by combining wave model and satellite data, J. Geophys. Res., 115, C03 020, https://doi.org/10.1029/2009JC005534, 2010.

Villas Bôas, A. B. and Young, W. R.: Integrated observations and modeling of winds, currents, and waves: requirements and challenges for the next decade, J. Fluid Mech., 890, R3, https://doi.org/10.1017/jfm.2020.116, 2020.

Villas Bôas, A. B., Ardhuin, F., Gommenginger, C., Rodriguez, E., Gille, S. T., Cornuelle, B. D., Mazloff, M. R., Bourassa, M., Subramanian, A., van Sebille, E., Li, Q., Fox-Kemper, B., Ayet, A., Mouche, A., Merrifield, S. T., Terrill, E. J., Rio, M. H., Brandt, P., Farrar, J. T., Fewings, M., Chapron, B., Shutler, J. D., and Tsamados, M.: Integrated observations and modeling of winds, currents, and waves: requirements and challenges for the next decade, 6, 425, https://doi.org/10.3389/fmars.2019.00425, 2019.

Villas Bôas, A. B., Cornuelle, B. D., Mazloff, M. R., Gille, S. T., and Ardhuin, F.: Wave-Current Interactions at Meso and Submesoscales: Insights fromIdealized Numerical Simulations, J. Phys. Oceanogr., in press, https://doi.org/10.1002/2016JC012413, 2020.

White, B. S. and Fornberg, B.: On the chance of freak waves at sea, J. Fluid Mech., 355, 113–138, 1998.

Appendix A: Ray equation in 1D

Let ~~'s~~ us consider a one dimensional stationary current shear: $\mathbf{u} = (\partial_x U x, 0)$. Starting from the ray equations in a Cartesian frame of coordinate (Mei, 1989; Phillips, 1977):

$$\partial_t k + \partial_x \omega = \cancel{0}0. \tag{A1}$$

ω is given by Eq. (2). The time derivative of the wavenumber k ~~, assuming that~~ is,

$$\partial_t k = -\partial_x \omega. \tag{A2}$$

Considering the intrinsic frequency constant ~~:~~ the Eq.(A2) becomes,

$$\partial_t k = -k\partial_x U. \tag{A3}$$

~~Which yield to :~~

$$2\partial_t \omega = -\omega \partial_x U$$

~~As the wave action is conserved:~~ We assume that $\partial_t \omega \sim \partial_t (gk)^{1/2}$. Here we have to derive a function composition. We obtain $\partial_t \sigma = \sqrt{\frac{g}{k}} 2\partial_t k$. Knowing that the phase speed ($\frac{\omega}{k}$) of waves in deep water is equal to ($\sqrt{\frac{g}{k}}$) it yields:

$$\frac{E(\sigma,\theta)}{\sigma} 2\partial_t \sigma = Cte - \sigma\partial_x U. \tag{A4}$$

~~H_s is function of wave action (Eq.(4)), hence, wave height gradient (∇H_s) can be written:~~

$$\nabla(\frac{H_s}{\sigma}) = 0$$

From Eq.1, assuming stationary condition and that the group speed is much bigger than the current speed

$$\nabla.(\mathbf{C}_g N) = 0 \tag{A5}$$

~~Thanks to~~ As $C_g = \frac{1}{2} C_\phi$ with $C_\phi = \sigma/k$, the Eq.A5 becomes,

$$\frac{\sigma}{2k\sigma} \frac{E(\sigma)}{\sigma} = Cte. \tag{A6}$$

The constant Cte depends on the initialization of the waves at the left boundary. From Airy theory for waves in deep water combined with Eq.4, one can find that $\frac{H_s^2 g}{4\sigma^2}$=Cte, and so,

$$\frac{H_s}{\sigma} = Cte' \tag{A7}$$

Taking the gradient of the Eq.(A7) combined with Eq.(A1~~) and knowing that $\partial_k \omega = C_g$, with C_g the wave train group velocity~~,A3) the constant of Eq.(A7) becomes null and we can write the gradient of the significant wave height as a function of the surface current gradient.

$$\nabla H_s \sim \frac{\partial_x U (H_s k)}{\sigma} \tag{A8}$$

Competing interests. Authors declare no conflict of interest in these works.

Author contributions. G.M designed the experiments, performed the numerical simulations and led the analysis of the results and writing. C.d.M provide the surface current fields used as the wave model forcing and contributed to the writing.

Acknowledgements. This work could not have been realized without the original idea proposed by Dr. Ana B. Villas Bôas, authors want to sincerely thank her. Also authors want to thanks their respective funders, G.M is supported both by the Centre National d'Etude Spatiale, focused on SWOT mission and the Region Bretagne through ARED program. C.d.M is funded by Direction Générale de l'Armement (DGA). Simulations were performed using the HPC facilities DATARMOR of "Pôle de Calcul Intensif pour la Mer" at Ifremer, Brest, France. We gratefully acknowledge B. Chapron for his helpful theoretical guidance. Finally authors ~~acknowledge~~ thank their respective Ph.D supervisors F. Ardhuin and X. Carton for their thesis guidance all along the past few years.